Research Paper

PAIN®

A phenotypic screening platform for chronic pain therapeutics using all-optical electrophysiology

Pin W. Liu[a], Hongkang Zhang[a], Christopher A. Werley[a], Monika Pichler[a], Steven J. Ryan[a], Caitlin L. Lewarch[a], Jane Jacques[a], Jennifer Grooms[a], Jean Ferrante[a], Guangde Li[a], Dawei Zhang[a], Nate Bremmer[a], Adam Barnett[a], Romina Chantre[a], Amy E. Elder[a], Adam E. Cohen[b], Luis A. Williams[a], Graham T. Dempsey[a], Owen B. McManus[a,*]

Abstract

Chronic pain associated with osteoarthritis (OA) remains an intractable problem with few effective treatment options. New approaches are needed to model the disease biology and to drive discovery of therapeutics. We present an in vitro model of OA pain, where dorsal root ganglion (DRG) sensory neurons were sensitized by a defined mixture of disease-relevant inflammatory mediators, here called Sensitizing PAin Reagent Composition or SPARC. Osteoarthritis-SPARC components showed synergistic or additive effects when applied in combination and induced pain phenotypes in vivo. To measure the effect of OA-SPARC on neural firing in a scalable format, we used a custom system for high throughput all-optical electrophysiology. This system enabled light-based membrane voltage recordings from hundreds of neurons in parallel with single cell and single action potential resolution and a throughput of up to 500,000 neurons per day. A computational framework was developed to construct a multiparameter OA-SPARC neuronal phenotype and to quantitatively assess phenotype reversal by candidate pharmacology. We screened ~3000 approved drugs and mechanistically focused compounds, yielding data from over 1.2 million individual neurons with detailed assessment of functional OA-SPARC phenotype rescue and orthogonal "off-target" effects. Analysis of confirmed hits revealed diverse potential analgesic mechanisms including ion channel modulators and other mechanisms including MEK inhibitors and tyrosine kinase modulators. Our results suggest that the Raf-MEK-ERK axis in DRG neurons may integrate the inputs from multiple upstream inflammatory mediators found in osteoarthritis patient joints, and MAPK pathway activation in DRG neurons may contribute to chronic pain in patients with osteoarthritis.

Keywords: Optogenetics, Electrophysiology, Drug discovery, Phenotypic screen, Osteoarthritis, Machine learning, Neurobiology

1. Introduction

Pain remains the primary reason patients seek medical care.[102] Chronic pain is difficult to treat, leading to significant morbidity, loss of productivity, and lower quality of life.[23,57,93] Among chronic pain indications, osteoarthritis (OA) is particularly prevalent,[42,55,60,75] with >30 million patients with OA in the United States, representing about one-third of the total chronic pain population.[95] Osteoarthritis and other forms of chronic pain are widely treated with opioids, but long-term use is limited by the occurrence of mechanism-based adverse effects, tolerance, and dependency, leading to a major health crisis in the United States.[36] Gabapentinoids, carbamazepine and nonsteroidal anti-inflammatory agents provide relief for only a subset of patients.[39] Despite the clear unmet medical need and significant research activity, few effective nonopioid drugs for OA pain have appeared in the past 2 decades.

A major factor limiting development of pain therapeutics is the lack of scalable, translatable models of sensory neuron function, which is essential for transmission of pain signals from the periphery to the brain.[46] Traditional approaches rely on target-based high-throughput screens, often under conditions that do not mimic physiological environments, followed by in vivo evaluation using animal pain models that often do not translate clinically.[35] Assays based on cell-based models have traditionally suffered from severe tradeoffs between throughput and information content.

Here, we address this need through development of a high-throughput all-optical electrophysiology platform focusing on an OA "pain-in-a-dish" model in rat dorsal root ganglion (DRG) neurons sensitized with OA-SPARC (OA-derived Sensitizing PAin Reagent Composition). The OA-SPARC is a formulation of inflammatory mediators found at elevated levels in synovial fluid of arthritic joints of patients.[77] To enable high-throughput screening, we used simultaneous optical stimulation and optical recording of neuronal action potentials (APs) with genetically encoded actuators and voltage indicators.[43] We previously developed the Firefly, a multi-well plate compatible wide-field microscope for optogenetic recordings from hundreds of neurons simultaneously with millisecond temporal resolution and single-cell spatial resolution.[116,117] This system maintains the rich information of manual patch clamp voltage

Sponsorships or competing interests that may be relevant to content are disclosed at the end of this article.

P. W. Liu, H. Zhang, and C. A. Werley contributed equally to this work.

[a] Quiver Bioscience, Cambridge, MA, United States, [b] Department of Chemistry and Chemical Biology, Harvard University, Cambridge, MA, United States

**Corresponding author. Address: Quiver Bioscience, 150 Cambridgepark Dr, Cambridge, MA 02140, United States. Tel.: 617-945-5433. E-mail address: owen.mcmanus@quiverbioscience.com (O. B. McManus).*

Supplemental digital content is available for this article. Direct URL citations appear in the printed text and are provided in the HTML and PDF versions of this article on the journal's Web site (www.painjournalonline.com).

PAIN 00 (2023) 1–19

http://dx.doi.org/10.1097/j.pain.0000000000003090

measurements and achieves >30,000-fold higher throughput. Using diverse stimulation patterns, we extract hundreds of electrophysiological features per neuron. Osteoarthritis-sensitizing pain reagent composition application drives a strong, multiparameter hyperexcitability phenotype in cultured DRG neurons and causes pain in vivo when injected into a rat hind paw.

We pharmacologically validated the model by showing phenotype reversal with clinical analgesics and expected responses to potent and selective tool compounds with diverse targets. We performed a phenotypic screen of ~3000 FDA-approved and mechanistically focused compounds to identify potential analgesic targets. Analysis of confirmed hits revealed known analgesic mechanisms (eg, ion channel modulators) and less well-characterized mechanisms (eg, mitogen-activated protein kinase inhibitors). Combining high-throughput optical electrophysiology with a rationally designed pain sensitization model enabled detailed phenotypic measurements for drug discovery in pain-relevant models of sensory neuron function. This platform promises to be more informative and relevant to human physiology than heterologous expression models, and faster, cheaper, and more quantitative than in vivo models.

2. Materials and methods

2.1. Solutions

2.1.1. Dorsal root ganglion dissection and culture media

2.1.1.1. Dissection media

Calcium and Magnesium Free HBSS (Fisher Scientific Waltham, MA) supplemented with 10 mM HEPES (Fisher Scientific) and 0.5× Penicillin-Streptomycin Solution (Corning), pH 7.35.

2.1.1.2. Plating media

DMEM/F12 medium (Fisher Scientific) supplemented with 10% heat-inactivated FBS (VWR), 10 mM HEPES (Fisher Scientific), and 0.5× Penicillin-Streptomycin Solution (Corning, Corning, NY), pH 7.35.

2.1.1.3. Culture media

BrainPhys Neuronal media (STEMCELL Technologies, Vancouver, Canada) supplemented with 1× N2 Supplement-A (Fisher Scientific), 1× SM1 Neuronal supplement (Fisher Scientific), 1× GlutaMAX (Fisher Scientific), 20 nM Trans-Retinel (Sigma-Aldrich, St. Louis, MO), 0.5× Penicillin-Streptomycin Solution (Corning), 2 ng/mL mouse GDNF (Sigma-Aldrich), 4 ng/mL human NT-3 (Sigma-Aldrich), and 1 μg/mL laminin (Fisher Scientific), pH 7.35.

2.1.2. Imaging buffer (in mM)

One hundred fifteen NaCl, 18 Na gluconate, 3 KCl, 1.1 $CaCl_2$, 1 $MgSO_4$, 0.5 Na_2HPO_4, 0.45 NaH_2PO_4, 4 D-glucose, 10 HEPES, and 0.15 Na pyruvate, pH 7.35.

2.2. Preparation of cultured dorsal root ganglion neurons

2.2.1. Plate preparation

Greiner cycloolefin (CO) half-area 96-well plates (Greiner Bio-one, Kremsmünster, Austria item no.: 675801) were plasma-treated for 3 minutes at 0.26 Torr with air (oxygen) plasma to make the surface hydrophilic. Plates were then sterilized by exposure to UV light in a tissue-culture hood for 30 minutes. Two days before plating of DRG neurons, wells were coated with 100 μg/mL poly-D-lysine (Sigma-Aldrich) in water and incubated at 4°C overnight. One day before plating of DRG neurons, wells were washed with PBS and coated with 20 μg/mL laminin (Fisher Scientific) in PBS and incubated at 4°C overnight. On the day of plating of DRG neurons, plates were retrieved and equilibrated to room temperature. Immediately before plating DRGs, laminin was aspirated, and wells were washed with plating media. From one rat litter, we routinely plated 7 full 96-well plates.

2.2.2. Cell preparation

Dorsal root ganglion neurons were prepared from Sprague-Dawley (SD) rats, postnatal day 10. Animals were anesthetized by using CO_2 inhalation and decapitated, and ganglia were removed. Dorsal root ganglia from one litter of 10 pups were treated at 37°C for 30 minutes in 2 mg/mL collagenase (type IA; Sigma-Aldrich) and 5 mg/mL dispase II (Sigma-Aldrich) in dissection media and then washed with and placed in plating media. Individual cells were dispersed by trituration with a fire-polished Pasteur pipette and filtered through 100-μm cell strainer. Cells were then counted and plated at a density of 2000 cells/well on Greiner half-area 96-well plates with a CO bottom (Greiner Bio-one, item no.: 675801) in plating media. cyclic olefin copolymer (COC), which was optimized for ultraviolet light applications, also makes substrate autofluorescence and laser-generated sample heating negligible upon red laser illumination.[78] The small well area conserves cells (2000 cells/well) and enables imaging of nearly the full well area. During cell preparation and culture maintenance, we used semi-automated culture with the Integra VIAFLO 96-channel pipettor, which reproducibly defines pipette location (*x*, *y*, and *z*) and injection/aspiration velocity.[78]

2.2.3. All-optical electrophysiology construct transduction

One hour after cell plating, Lenti-X Concentrator concentrated lentiviruses including CaMKII-CheRiff-EBFP2 and CaMKII-QuasAr3-Citrine were added for transduction. Cells were then incubated in a cell culture incubator with 5% CO_2 at 37°C overnight. Sixteen to eighteen hours after transduction, virus was removed, and cells were fed with culture media until compound treatment.

2.2.4. Cell culture maintenance and compound treatment

The OA-SPARC stock solution was prepared at 1000× (see recipe in **Table 1**), aliquoted, and stored at −80°C. Compounds were prepared at 200× in DMSO and stored at −20°C. Twenty-four hours before imaging, OA-SPARC and compounds were diluted in culture media and added to the cells at the assay concentration. Thirty minutes before imaging, culture media was aspirated from the wells and OA-SPARC and compounds were prepared in imaging buffer and added to the cells using Perkin Elmer JANUS Mini automated liquid handling system.

2.3. All-optical electrophysiology imaging

Imaging experiments were performed 5 days after DRG neuron plating into 96-well plates. Before imaging, the cells were first washed with imaging buffer then treated with OA-SPARC and tested compounds using a PerkinElmer Janus Mini liquid handling robot. Cells were then incubated for 30 minutes at 27°C. Imaging experiments were performed on the Firefly microscope equipped with an automated stage (Ludl Bio-Precision2; Ludl Electronic Products, Hawthorne, NY) at 27°C. Briefly, QuasAr3 voltage sensor was illuminated by 2 red lasers

Table 1

Optimized formulation of osteoarthritis-sensitizing pain reagent composition.

Ingredient	Abbreviation	Conc. (pM)	Gene name (rodent)	Rat receptor gene description	Mean TPM	SD TPM	Expression description	Expression range
Nerve growth factor	NGF	10	Ngfr	Nerve growth factor receptor	285.8	30.3	Medium	Medium
			Ntrk1	Neurotrophic receptor tyrosine kinase 1	49.5	2.3	Medium	
Tumour necrosis factor alpha	TNFα	0.3	Tnfrsf1a	TNF receptor superfamily member 1A	149.7	5.8	Medium	Low-medium
			Tnfrsf1b	TNF receptor superfamily member 1B	5.9	0.8	Low	
Interleukin 6	IL-6	20	Il6r	Interleukin 6 receptor	9.8	0.4	Low	Low-medium
			Il6st	Interleukin 6 cytokine family signal transducer	104	3.5	Medium	
Bradykinin	BK	500	Bdkrb1	Bradykinin receptor B1	0.1	0.1	Absent	Absent-medium
			Bdkrb2	Bradykinin receptor B2	19.1	0.5	Medium	
Interleukin 1 beta	IL-1β	8	Il1r1	Interleukin 1 receptor type 1	10.3	0.4	Low	Low-medium
			Il1rap	Interleukin 1 receptor accessory protein	27.9	1.2	Medium	
Interleukin-17	IL-17	0.1	Il17ra	Interleukin 17 receptor A	17.1	0.9	Medium	Low-medium
			Il17rb	Interleukin 17 receptor B	1.2	0.2	Low	
			Il17rc	Interleukin 17 receptor C	12.2	1.1	Medium	
			Il17rd	Interleukin 17 receptor D	4.2	0.3	Low	
			Il17re	Interleukin 17 receptor E	1.1	0.2	Low	
Prostaglandin E2	PGE2	8000	Ptger1	Prostaglandin E receptor 1	14.8	0.9	Medium	Low-medium
			Ptger2	Prostaglandin E receptor 2	4.5	0.7	Low	
			Ptger3	Prostaglandin E receptor 3	11.9	0.9	Medium	
			Ptger4	Prostaglandin E receptor 4	2	0.1	Low	
CC Motif chemokine ligand 2	CCL2	30	Ccr2	C-C motif chemokine receptor 2	0	0.1	Absent	Absent-low
			Ccr3	C-C motif chemokine receptor 3	0	0	Absent	
			Ccr5	C-C motif chemokine receptor 5	1	0.1	Low	
Vasoactive intestinal peptide	VIP	3	Adcyap1r1	ADCYAP receptor type I	1.7	0.3	Low	Absent-low
			Vipr1	Vasoactive intestinal peptide receptor 1	0.1	0.1	Absent	
			Vipr2	Vasoactive intestinal peptide receptor 2	0.8	0.1	Low	
Reference (marker gene)	Marker		Scn9a	Sodium voltage-gated channel alpha subunit 9	24.6	1.9	Medium	Low-medium
			Scn10a	Sodium voltage-gated channel alpha subunit 10	14.9	0.5	Medium	
			Scn11a	Sodium voltage-gated channel alpha subunit 11	13.2	1.1	Medium	
			Trpv1	Transient receptor potential cation channel subfamily V member 1	7.7	0.9	Low	

Concentrations shown are at top of the range measured in patients. Expression levels of genes are quantified using transcript per million (TPM) values of these genes in vehicle-treated cultured rat DRG samples. The expression of each gene is categorized as absent (<0.5 TPM), low (<11 TPM), medium (<1000 TPM), or high. The expression of genes for each ingredient is summarized based on the expression of each gene.

(638 nm, 8 W; DILAS-Coherent, Santa Clara, CA). Laser light was homogenized and refracted onto the sample via near-TIR illumination (NA 0.4, UPlanSApo 10×/0.4; Olympus, Shinjuku City, Tokyo) at a light intensity around 120 W/cm^2. Blue light for optogenetic stimulation was projected by a high-power LED (462 nm, 6.2W; Luminus Devices Inc, Sunnyvale, CA) via a fast digital mirror device (DMD) (Vialux, Chemnitz, Germany) through an objective lens (NA 0.5, 2×/0.5 MV Plapo 2XC; Olympus, Shinjuku City, Tokyo) onto the sample. QuasAr3 fluorescence was filtered by a 736/128 nm bandpass filter and detected by a CMOS camera (ORCA-Flash4.0; Hamamatsu, Bridgewater, NJ). To achieve a frame rate of 500 Hz, data were acquired with a center camera chip of 800 × 160 pixels at 2 × 2 pixel binning, which corresponds to the 4 × 0.8 mm recording area in the well.

Each well was typically stimulated with a protocol consisting of 2 long pulses (11.25 and 58 mW/cm^2, 500 ms each), 8 short pulses (2.44, 5.5, 9.43, 14.67, 22, 33, 51.33, and 88 mW/cm^2, 100 ms each), followed by a linear conductivity ramp pulse (0.125-30 mW/cm^2 for 2.5 seconds) of blue light (**Fig. 1B**). The stimulus protocol lasted a total of 8.5 seconds.

Scanning progressed from well A1 to well A12, then B12 to B1, then C1 to C12, and so on until in well H1, in a column-wise serpentine pattern, then reversed from H1 to H12, then G12 to G1, then F1 to F12, and so on until back to well A1, in a reversed column-wise serpentine pattern, then in the column-wise serpentine pattern again, ie, from A1 to A12, then B12 to B1, then C1 to C12, and so on until in well H1. Using this serpentine–reversed serpentine–serpentine pattern reduced the time-on-microscope effect. A complete 96-well plate required 67 minutes to scan using this protocol.

2.4. Small molecule library

A library of approximately 2400 approved drugs was assembled from 4 commercial sources (Prestwick, Enzo, ApexBio, and TargetMol). These drugs had been approved by regulatory agencies in the United States, Canada, European Union, Japan, and other countries. Because of duplications across individual libraries, this collection of approved drugs was contained in ~3400 individual wells. This library was supplemented with a series of annotated libraries from Biomol containing 842 additional compounds that target a variety of CNS signaling/regulatory mechanisms and expressed proteins including endocannabinoids, ion channel ligands, adrenergic ligands, dopaminergic ligands, opioid ligands, cholinergic ligands, histaminergic ligands, ionotropic glutamatergic ligands, metabotropic glutamatergic ligands, GABAergic ligands, purinergic ligands, kinase inhibitors, and phosphatase inhibitors.

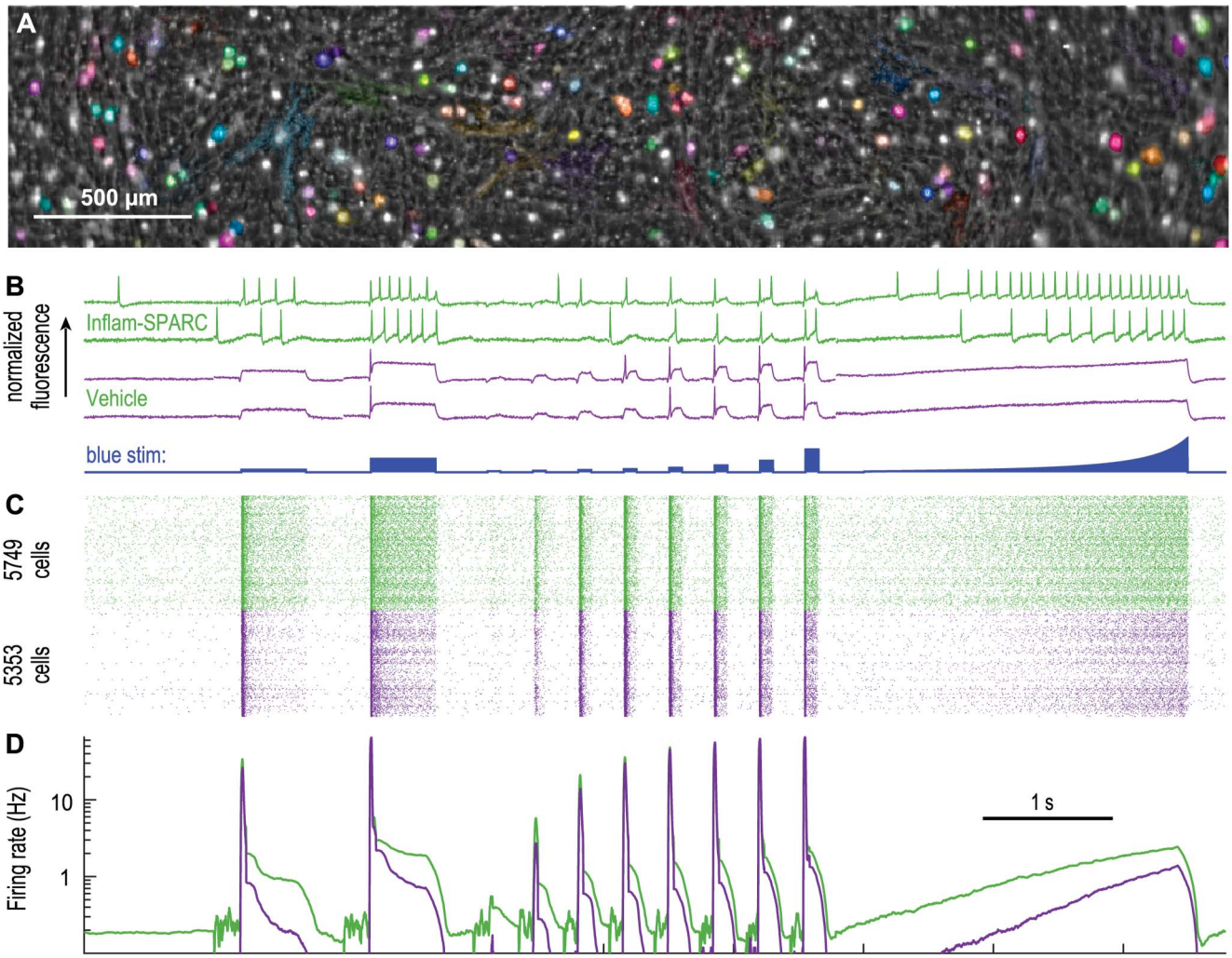

Figure 1. High-throughput measurements of sensory neuron excitability using all-optical electrophysiology. Rat dorsal root ganglion (DRG) neurons were dissected from P10 animals, cultured 5 days in 96-well plate format and activity recorded using the Firefly instrument. (A) Firefly image of DRG neurons with colored overlays of spiking cells identified by automated analysis. Different colors correspond to unique individual cells. (B) Example voltage recordings showing behaviors in response to step and ramp optogenetic stimuli (blue). Neurons are recorded from 2 conditions: vehicle control (purple) and treatment with inflammatory Sensitizing PAin Reagent Composition or SPARC ("Inflam-SPARC"), a cocktail of inflammatory mediators designed to model inflammatory "pain-in-a-dish." The formulation of Inflam-SPARC is (nM): 0.5 bradykinin, 100 serotonin, 100 histamine, 20,000 ATP (adenosine triphosphate), and 10 prostaglandin E2. (C) Raster plot where each row within a color is one neuron and each point is an identified action potential. The data are pooled from 3 fields of view (FOVs) in each of 32 wells. In total, >5000 neurons were recorded for each condition with single cell and single action potential resolution in a single imaging session. (D) The spike rate averaged over active cells. The increased firing rate induced by the Inflam-SPARC is clearly visible, both in the raster plot and in the associated elevated spontaneous and evoked firing rates.

2.5. Osteoarthritis-sensitizing pain reagent composition in vivo validation

In vivo validation studies were conducted at Pharmaron Beijing Co, Ltd. (Beijing City, China). Male and female SD rats with age 6 to 8 weeks were kept in laminar flow rooms at constant temperature and humidity with 3 animals in each cage. Rats were housed in a polycarbonate cage with a 12:12 hours of light/dark cycle and in an environmentally monitored, well-ventilated room maintained at a temperature of 22 ± 3°C and a relative humidity of 40% to 80%. Food and water were available ad libitum. Animals were quarantined for 5 days before the study. The general health of the animals was evaluated by a veterinarian, and complete health checks were performed. Animals with abnormalities were excluded before the study. After 5 days of acclimatization to the environment, the body weights of all the rats were recorded before dosing with a total number of 5 male and 5 female rats in each test group (5 groups in total). Rats were randomly assigned to respective groups using a computer-generated randomization procedure. At the time of the compound dosing, the body weight of the rats was 189 to 218 g for male rats and 155 to 192 g for female rats. Vehicle (PBS), complete Freund adjuvant (CFA) or OA-SPARC (80×, 400×, and 2000×) dissolved in PBS was injected into the left hind paw (50 µL per injection). Weight-bearing and von Frey threshold measurements were performed 5 times during the study, including baseline before dosing (−1 hour) and 1, 8, 24, and 72 hours after dosing to evaluate the effects of each test agent in a blinded manner.

For the von Frey test, mechanical allodynia of the left hind paw was measured by determining withdrawal thresholds to an electronic von Frey filament (Bioseb, Vitrolles, France). The filament was applied perpendicularly to the plantar surface of the paw with increasing force. The force required to induce a reflex paw withdrawal was calculated by taking the average of 2 to 3 repeated stimuli (in grams), which induced a reflex paw withdrawal. For the weight-bearing test, rats were tested in a weight balance changing instrument (YLS-11A; JinanYiYan Science and Technology

Development Co, Ltd) constructed to register the weight load exerted by the hind paws by means of force plates inserted in the floor. The unequal weight distribution between the dose–injection and contralateral paw (in grams) was determined in 10 seconds. One-way analysis of variance (ANOVA) was applied to estimate main effects, and *P*-values were adjusted by multiple comparison correction using software SPSS 16.0, and $P < 0.05$ was accepted as significant. The technicians were blind to treatment during the study. The testing order of subjects with respect to treatment was counterbalanced across time of day to avoid all of one treatment being tested in the first part of the day. For the assessment of a test compound, where possible, an entire cage was randomized with representative samples from each treatment group or dose level. An excel spreadsheet was created that listed the assigned subject ID to each test session, observation arena, treatment group (blinded), the pretreatment time, the test time, the details of the environment, and a comments section to document any unexpected events (eg, mis-injection).

2.6. Analysis

2.6.1. Analysis pipeline

Movies were recorded serially from each plate and the typically 100s of Gigabytes of data were transferred to Amazon Web Services (AWS) for storage and parallelized analysis. Using a watershed algorithm based on the movie mean frame, each field of view (FOV) was divided into regions that were individually segmented to find sources. Patch-wise Principal Component Analysis (PCA)/Independent Component Analysis (ICA)[73] was used to find spatiotemporally correlated fluorescence signals. The patches were then merged, and sources were combined or split. The temporal covariance of pixels for each cell was used to generate an "activity mask," consisting of the pixels that correspond to that cell and weights for each pixel. Single-cell voltage-time traces were computed using the mask to calculate a weighted average of those pixels for each frame in the movie.

Before feature extraction, corrections for photobleaching and crosstalk were computed and applied. The photobleaching effect was estimated for each imaging epoch by fitting a linear plus exponential curve to the unstimulated portions of each epoch and then interpolating to the whole epoch. "Crosstalk" refers to a small amount of fluorescence elicited directly by the blue light used for optogenetic stimulation. Based on the known optical properties of the 2 illumination sources (red laser and blue LED) and the optical filters in the Firefly imaging system, we estimated the blue light stimulation-induced crosstalk. After each trace was corrected, spike detection was performed to identify action potentials using a kernel-based method that starts with reasonable priors for the shape of a spike and optimizes the kernel for each neuron. For each cell, a total of 560 features were computed that summarize the shape and timing of action potential firing as a function of stimulus intensity and duration. This detailed parameterization made the assay sensitive to subtle perturbations of neuronal function. Cells were scored based on morphological properties such as size and connectivity of the cell bodies as well as signal-to-noise ratio (SNR) of the detected spikes, and cells with a low score (eg, SNR < 3) were discarded. Results were loaded into a database, from which feature tables were generated for further analysis.

2.6.2. Time bin analysis

Based on the diverse stimulation protocol, each movie was split into 46 time bins covering different portions of the protocol. Firing frequency and 3 spike shape parameters (spike height, width, and after-hyperpolarization) were aggregated for each cell across each bin. This yielded 184 additional features that captured diverse aspects of cellular behavior under various stimulation scenarios with a granularity not found in the other precomputed features.

2.6.3. Inflam-sensitizing pain reagent composition exploratory analysis

Thirty-two wells each of Inflam-SPARC and vehicle conditions were available for each sentinel plate. A *t* test (unpaired assuming equal variance) was performed for all the features. A false discovery rate (FDR)-based multiple testing correction method was then applied to adjust the *t* test–derived *P*-values.[9] Then the adjusted *P*-values were ranked based on the most significant difference between the vehicle and Inflam-SPARC groups. A significant ($P < 0.01$) and diverse subset of 8 features, covering both spike shape and spike timing features at different blue light stimulation epochs, was manually selected for visualization of the effect of Inflam-SPARC on the cell population.

2.6.4. Osteoarthritis-sensitizing pain reagent composition phenotyping

The analysis pipeline extracted 744 features describing action potential shape and timing in response to diverse optogenetic stimuli (560 features from the analysis pipeline and 184 features from time bin analysis). To focus our downstream analysis on physiological features relevant to pain, we identified a subset of features that had a strong and reliable response to OA-SPARC treatment. Features were selected based on a statistically consistent OA-SPARC signal across 5 rounds of cell plating and imaging. Each round consisted of 3 plates with 32 wells each for OA-SPARC and control conditions (a typical well contains 100-300 individual DRG neurons). First, for each of the 744 features, linear mixed effects models[6] were used to estimate *P*-values for the difference between OA-SPARC and control conditions in a way that was sensitive to hierarchical sources of experimental variance. A false discovery rate correction was performed to correct for multiple comparisons. Physiological features that had significant *P*-values after adjustment (adjusted *P*-value < 0.05) in all 5 rounds of measurement were passed on to a LASSO regression,[111] which automatically performs feature selection by setting coefficients of nonrelevant features to zero. Around 40 features survived this selection process. An additional process of manual selection was applied to select features with the lowest correlation to other selected features and with clear connections to established electrophysiological parameters while keeping a stable phenotypic window across imaging rounds. This procedure yielded 8 features used to describe the OA-SPARC phenotype.

These features were combined using a principal components analysis to account for covariance. We then used vector decomposition to compute a single disease score: in the principal component space, an average disease vector was defined that points from the average of all OA-SPARC wells to the average of vehicle-treated (no SPARC) wells. The position vector for each individual well was projected onto the average disease vector, and the length of the projection, which describes activity along the desired direction in the principal component space, was called the phenotype score. A total distance score, defined as the distance of a given well from the average of vehicle (no SPARC) wells, was also computed. This distance score is effectively Mahalanobis distance.[18] The Z' factor for the screen was defined

as $Z' = 1-3(\sigma_p + \sigma_n)/\left|(\mu_p - \mu_n)\right|$, where σ_p is the SD of the vehicle (no SPARC) wells, σ_n is the SD of the OA-SPARC–sensitized wells. μ_p is the mean of the vehicle (no SPARC) wells and μ_n is the mean of the OA-SPARC–sensitized wells. The on-target phenotype score consistently exhibited a $Z' > 0.2$ for the phenotyping plates and was used as the primary metric in the high-throughput drug screen and hit confirmation. The total distance score was used to evaluate confirmed hits in dose–response experiments.

2.6.5. Statistics

Except where otherwise noted, values reported in text were computed by first computing an average value for all neurons in a single well (eg, average firing frequency under gentle stimulation), and then reporting a mean, SD, or SE over replicate wells. Radar plots illustrate effect size on the radial axis using a metric called the common language effect size (CLES).[66] The intuition for CLES is that, when comparing a test distribution to a reference distribution, the effect size is the probability that a random sample from the test distribution is larger than a random sample from the reference distribution. If the distributions are non-overlapping, that effect can be 0 (test < reference) or 1 (test > reference). The CLES of a distribution compared with itself is exactly 0.5.

2.7. RNA sequencing

Rat dorsal root ganglion cultures were largely prepared as described in section 2.2.2, but plated at a density of 5000 cells/well on Greiner full-area 96-well plates with a COC bottom (Greiner Bio-one, item no.: 655801). After 1 day of culture, cells were treated with 1× PBS. On day 8 of culture, wells were pooled (3 wells/sample) in TRIzol and stored at −80°C. RNA extraction was performed according to the manufacturer's specifications for TRIzol extraction (ThermoFisher Scientific, Waltham, MA). Library preparation (mRNA profiling using poly-A selection) was performed using NEBNext Ultra II RNA Library Prep Kit for Illumina using the manufacturer's instructions (NEB, Ipswich, MA). 2× 150 bp paired end sequencing was performed on an Illumina HiSeq 4000. Demultiplexing was performed using bcl2fastq (v2.17) with one mismatch allowed for index identification. Reads were trimmed to remove Illumina adapter sequences and low-quality sequences using Trim Galore! (v.0.6.6, CutAdapt v2.8, default settings). Salmon (v.1.5.1, default settings) pseudo-alignment and quantification was performed against a rat reference transcriptome (RefSeq GCF_015227675.2_mRatBN7.2) built with recommended genomic decoys. Count and TPM tables were imported into R (3.6.2) and summarized to gene-level values using tximport (1.14.2). The qualitative assessments of gene-level expression (absent/low/medium) were based on cut-offs from the EMBL-EBI expression atlas (https://www.ebi.ac.uk/gxa/FAQ.html), where <0.5 mean TPM was classified as absent, <11 mean TPM as low, and <1000 mean TPM as medium. Raw and processed data are available in GEO (accession GSE237797).

3. Results

3.1. High-throughput, single-cell measurements of sensory neuron excitability for assessing candidate pharmacology

We previously built an integrated technology platform combining cell-based models, custom instrumentation[43] for optogenetic recordings, and computational tools for high-throughput measurements of neuronal excitability[78,116,117] and synaptic transmission.[11,115] The engineered channelrhodopsin CheRiff enables neuronal stimulation with blue light and the engineered voltage-sensitive protein QuasAr3 enables high-speed fluorescence recordings of changes in membrane potential with red light.[123] Our wide field-of-view (FOV) *Firefly* microscope (0.8 × 4 mm) can stimulate any subset of neurons with a fully configurable optical pattern using a digital micromirror display and simultaneously record voltage from the entire FOV with a single-cell spatial resolution, millisecond temporal resolution, and a signal-to-noise ratio (SNR, spike height: baseline noise) of approximately 9.5 (95% CI: 4.58-20.3). Custom software and analysis tools handle the high-speed voltage imaging data. The Firefly system has been applied to many types of rodent primary neurons and human induced pluripotent stem cell–derived neurons.[51,117]

Here we extended our approach to in vitro cultures of rodent DRG sensory neurons. Rat DRG neurons were cultured in 96-well plates, and optogenetic constructs were introduced through lentiviral delivery. Movies were then recorded serially, well-by-well on the *Firefly* microscope. Neurons within each FOV were interrogated with a varied stimulus pattern using blue light (470 nm) designed to probe a broad range of neurophysiological behaviors. We established an automated analysis workflow. After recording from each plate, primary data files were transferred to Amazon Web Services (AWS) for storage and hundreds of processors analyzed the movies in parallel to extract single-cell fluorescence-voltage traces. A typical 96-well plate produces ~300 GB of primary data that can be analyzed using cloud compute resources in ~1 hour. Results were loaded into an internal database for further analysis.

3.2. Platform validation using inflam-sensitizing pain reagent composition

We validated the platform using an established mixture of soluble mediators that occur in inflammatory pain,[5] here called "Inflam-SPARC." **Figure 1** shows optical voltage recordings from 11,102 individual neurons obtained from one-third of a 96-well plate. Two conditions are shown: (1) neurons treated with Inflam-SPARC[107] and (2) vehicle control-treated neurons. An FOV of ~100 DRG sensory neurons in the presence of supporting cells (**Fig. 1A**) was stimulated with a protocol that included short (100 ms) and long (500 ms) depolarization steps with various blue light intensities and a linear depolarizing ramp at the end (**Fig. 1B**, see Methods for detailed protocol). The soma diameter was estimated from the functionally determined masks of each cell; the median diameter of our recorded rat DRG neurons is around 27 μm, which is similar to literature report[4] (Supplementary Fig. S1, available at http://links.lww.com/PAIN/B942). Dorsal root ganglion neurons of all sizes were used in a combined analysis to derive phenotypes and evaluate compound pharmacology.

Individual cells were segmented using an activity-based algorithm. All the pixels capturing fluorescence from one neuron co-varied in time after the cell's unique firing pattern (**Fig. 1B**). This covariance was used to generate a weight mask for each cell (colored masks in **Fig. 1A**); pixels within each mask were averaged for each frame to calculate the single-cell voltage traces. From the traces, each action potential (AP) for each individual neuron in the dataset was identified and plotted in a raster graph (**Fig. 1C**), in which each row represents an individual recorded neuron, each column is a frame from the functional movies (~2 ms frame interval from 500 Hz recording), and each dot indicates a single identified action potential from that neuron.

Figure 1D represents a further compression of these data in a firing rate plot that summarizes the mean firing rate vs time from >5000 neurons from each condition shown in **Figure 1C**. The average number of spikes per frame is computed at each frame for each experimental group. These ratios are converted to spike rates by dividing by the sample duration producing a histogram of action potentials per 2 ms time bin per cell identified in recorded movies. The resulting time series is then smoothed using a variable-width kernel that is narrower where firing rates are higher, wider where they are lower. This curve is used only for summary data visualizations, and none of these computed features are used in quantifying cellular phenotypes.

The electrophysiological phenotype of applying Inflam-SPARC to DRG neurons includes a clear increase in AP firing during all epochs of blue light stimulation and particularly during sustained periods of lower-intensity stimulation (frequency increases from 1.09 ± 0.04 Hz in no SPARC to 2.04 ± 0.08 Hz in Inflam-SPARC at the first long pulse with stimulus power 11 mW/cm^2, mean ± SEM, $P < 0.001$). In addition, the optical rheobase (minimal blue light to initiate an AP) was significantly lowered by Inflam-SPARC (34 ± 2 mW/cm^2 in no SPARC to 9.4 ± 0.53 mW/cm^2 in Inflam-SPARC, mean ± SEM, $P < 0.001$), indicating enhanced excitability. The example traces in **Figure 1B** demonstrate the underlying variability in individual neuron behavior and illustrate the need to record from many hundreds or thousands of neurons to characterize subtle pharmacological effects. Additional representative traces for Inflam-SPARC and vehicle conditions from this experiment can be found in Supplementary Fig. S2 (available at http://links.lww.com/PAIN/B942). These measurements were made in a 96-well plate format yielding ~175 single-cell recordings per well.

3.3. Multidimensional analysis of electrophysiology for evaluation of disease and pharmacological phenotypes

An automated analysis pipeline was developed to process the large datasets for detailed phenotype characterization. The pipeline extracted spike timing properties (eg, spike frequency for each stimulus step, optical rheobase) (**Fig. 2A**) and spike shape parameters (eg, spike width, height, after-hyperpolarization, upstroke slope, and downstroke slope) (**Fig. 2B**) for each stimulus condition, yielding 560 parameters per neuron. We further subdivided the stimulus protocol into 46 time bins covering different portions of the protocol to capture aggregate behavior (**Fig. 2C**). Firing frequency and spike shape parameters were combined for each cell across each time bin, yielding 184 additional parameters that captured diverse stimulation-dependent activity patterns. This inclusive set of parameters was designed to capture all aspects of neuronal electrophysiology, although several of the parameters were redundant or strongly correlated with other parameters.

To summarize and visualize the effect of Inflam-SPARC on rat DRG neurons, we selected a set of 8 relevant parameters (see Methods section 2.6.3 for details) that are representative of the full phenotype for display in a "radar plot," including 5 spike timing properties from different epochs in the blue stimulus paradigm and 3 spike shape parameters in the ramp (**Fig. 2D** and Supplementary Fig. S3, available at http://links.lww.com/PAIN/B942). In all cases, a comparison between Inflam-SPARC and vehicle-treated conditions was significant ($P < 0.01$) after correction for multiple comparisons (*t* test, sample size, see Methods section 2.6.3). The difference between the Inflam-SPARC (green) and no SPARC (purple) radar plots represents the pain phenotypes. Our goal was ultimately to identify compounds

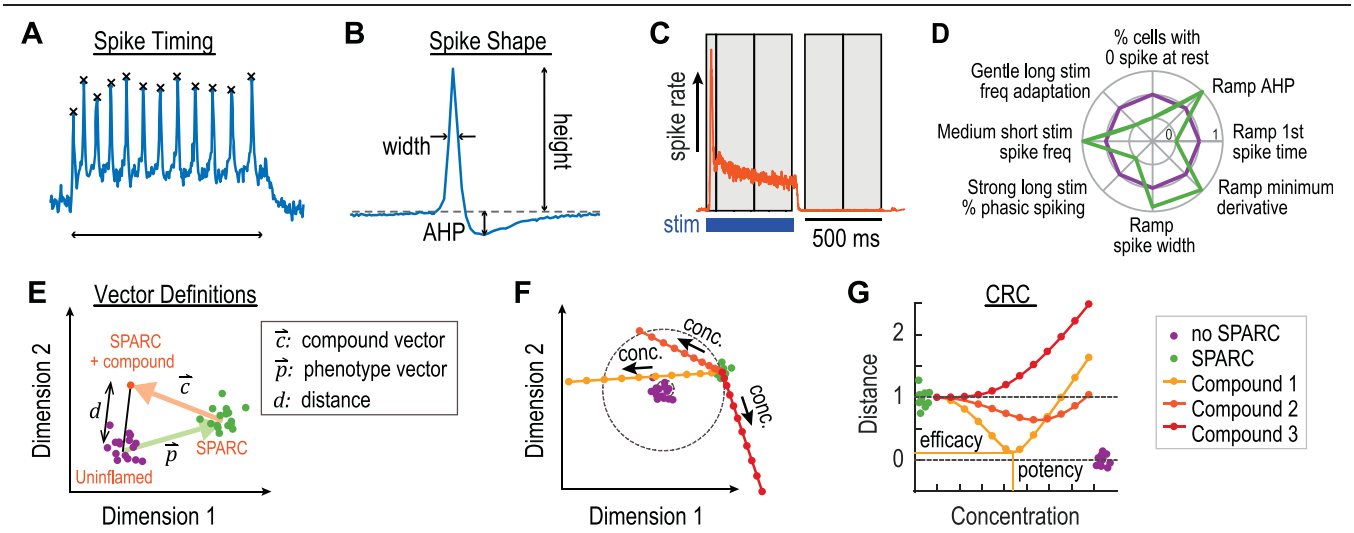

Figure 2. Quantitative characterization of DRG neuron activity in response to Inflam-SPARC revealed multidimensional phenotype. (A) Spike timing properties are automatically extracted including adaptation and maximum spike rate. (B) Spike shape properties are measured for each action potential, including after hyperpolarization (AHP). A total of 560 timing and shape parameters are extracted from each source trace. (C) The optogenetic stimulus protocol is broken into time bins (gray), and spike shape and timing information is aggregated from each bin, resulting in a 184-parameter vector describing neuronal function in different portions of the protocol. In total, this yields a 744-parameter dataset for each neuron. (D) The features with the most significant differences after Inflam-SPARC application are identified using statistical and machine learning tools, showing a multidimensional fingerprint of neuronal behavior. Each parameter is normalized to the uninflamed condition (purple). The pain phenotype induced by Inflam-SPARC is shown in green. (E) A diagram with mock data showing examples of well location in the multidimensional phenotype space (only 2 dimensions shown for clarity). No SPARC, uninflamed wells (purple), and SPARC-treated wells (green) form distinct clusters. A compound-treated SPARC well (orange) falls elsewhere in the space, and the Euclidean distance *d* between compound and no SPARC wells relative to the length of the phenotype vector *p* quantifies phenotype reversal and reflects compound efficacy. The compound vector *c* defines the vector between SPARC-treated wells and SPARC-treated wells in response to compound treatment. (F) Concentration–response compound trajectories showing 3 mock examples of potential responses; yellow values move toward phenotype rescue with overshoot at high concentrations; red values move orthogonally to the ideal compound rescue vector. (G) Concentration–response curve (CRC) corresponding to mock trajectories in (F). An ideal compound would reverse the inflammatory phenotype with very small distance (high efficacy) at low concentrations (high potency). DRG, dorsal root ganglion; SPARC, sensitizing pain reagent composition.

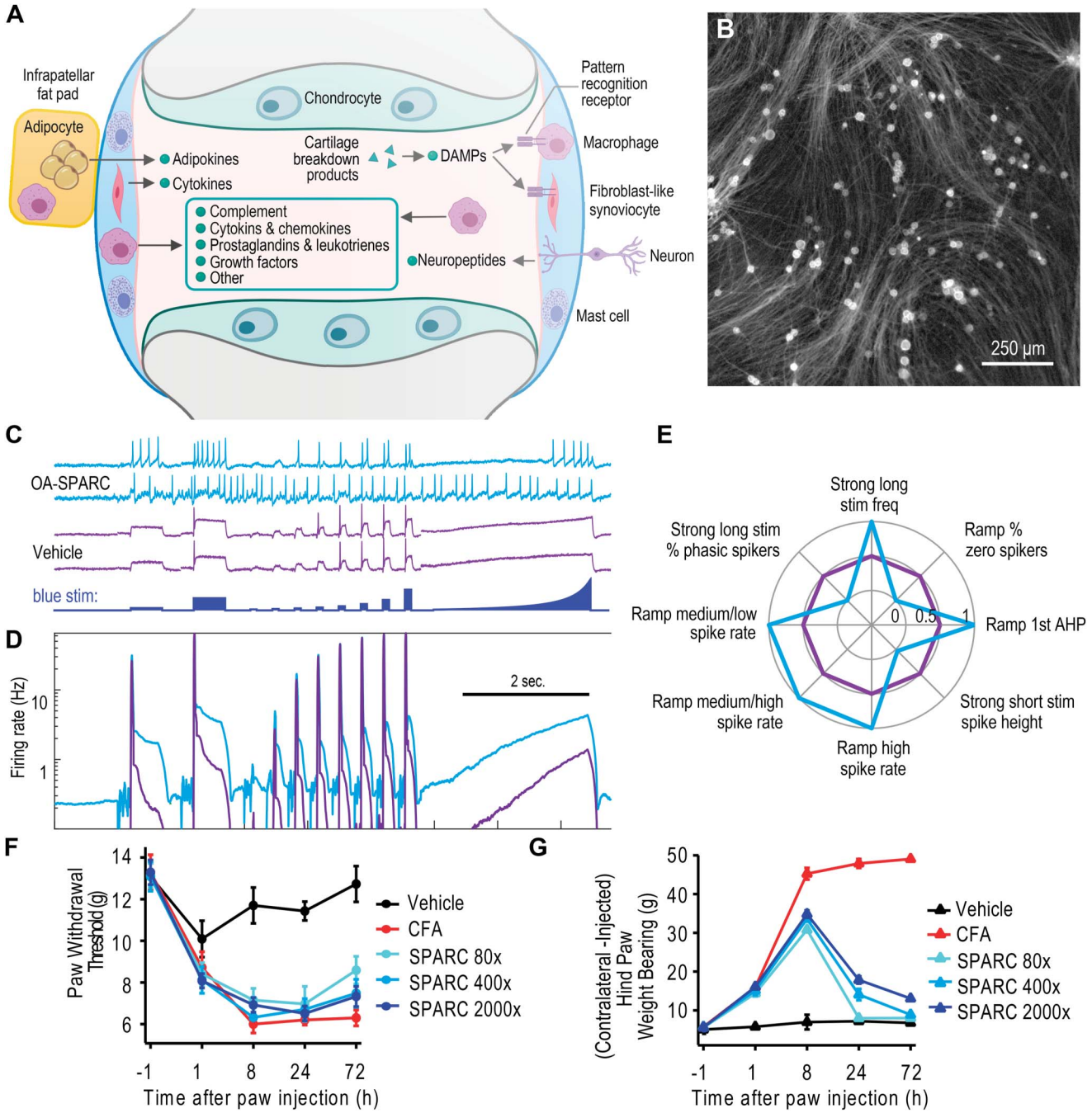

Figure 3. Design and validation of a SPARC for osteoarthritis (OA) pain. (A) Cartoon illustrating the complex cellular interplay in the synovial joint. In an osteoarthritic state, several inflammatory mediators are secreted into the synovial fluid of joints that leads to neuronal hyperexcitability and induced pain. (B) Rat DRGs were dissected from P10 rats, plated in 96-well plates, and transduced with viruses for optogenetic constructs 1 hour after plating. CheRiff-mOrange2 fluorescence ($\gamma = 0.5$ to highlight dim axons) is shown. The membrane-trafficked construct shows the extensive axonal processes in cultured rat DRG neurons, which contain many of the receptors that respond to OA-SPARC ingredients. (C and D) Neurons were treated with OA-SPARC for 24 hours. (C) Example optical physiology recordings in response to the optogenetic stimulation (blue) showed a significant increase in activity. (D) The population-averaged (>8000 neurons in total) firing rate was increased by treatment with OA-SPARC. The SPARC induced hyperexcitability in 3 ways: (1) increased spontaneous firing rate, (2) higher maximal firing rate under optogenetic stimulation, and (3) firing in response to a gentler stimulus (see, eg, left edge of ramp). (E) Salient features from the 744 parameters showing a significant and stable difference between the OA-SPARC and untreated conditions were identified using statistical approaches, yielding a multidimensional fingerprint of neuronal behavior. Each parameter was normalized to the uninflamed condition (purple). The pain phenotype induced by OA-SPARC is shown in blue. (F and G) OA-SPARC was injected into the hind paws of 6- to 8-week-old rats and leads to induced pain. Induced pain was compared against vehicle (negative control) and CFA (positive control). (F) The electronic von Frey test, where the paw was poked from below by a filament and the minimum force required to trigger paw withdrawal from the cage floor was recorded. (G) A weight-bearing test, where the weight placed on both injected and uninjected hind paws was recorded. Error bars are SD. AHP, after hyperpolarization; CFA, complete Freund adjuvant; DAMP, danger-associated molecular pattern; DRG, dorsal root ganglion; SPARC, sensitizing pain reagent composition.

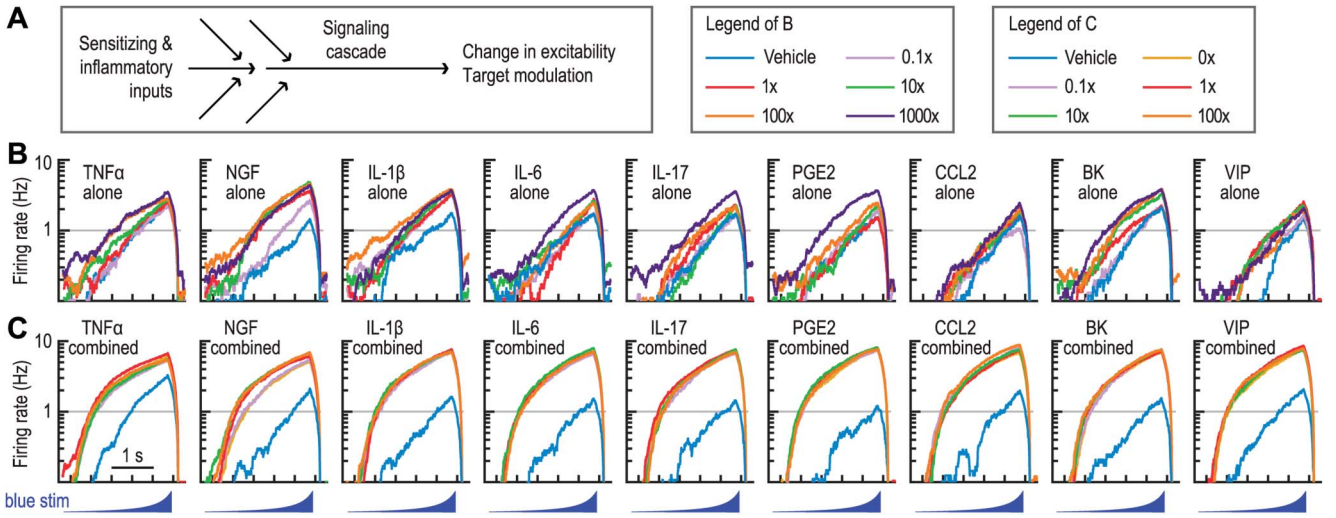

Figure 4. Concentration response of OA-SPARC ingredients individually and in combination demonstrated synergistic or additive effects from the combination of all components. (A) Diagram depicting inflammatory inputs from OA-SPARC that lead to a signaling cascade resulting in modulation of targets and changes in neuronal excitability. (B) The spike rate in response to a ramped stimulus (bottom). Each ingredient is titrated alone. (C) Each component is titrated in the presence of the other 8 ingredients, each at 10× concentration. The "vehicle" condition has no inflammatory mediators. All components have an effect alone, but the largest, most robust hyperexcitability phenotype is seen using the full formulation of components. Color legends for (B and C) are shown in the upper-right corner; 1× concentration is defined in Table 1. OA, osteoarthritis; SPARC, sensitizing pain reagent composition.

that reverse pain phenotypes, moving the inflamed DRG spiking behavior onto that of uninflamed DRGs. Parameter values in the radar plots can provide mechanistic information on effects of SPARCs and compounds on sensory neuron function. For example, the hyperexcitability induced by Inflam-SPARC is reflected by the reduced time to the first spike during the ramp stimulation (from 1.74 ± 0.04 seconds in no SPARC to 0.83 ± 0.04 seconds, mean ± SEM, in Inflam-SPARC; **Fig. 2D** "Ramp first spike time") and the reduced percentage of silent cells at rest during periods lacking optical stimulation (from 98 ± 0.1% in no SPARC to 91 ± 0.6%, mean ± SEM, in Inflam-SPARC; **Fig. 2D** "% cells with 1 spike at rest"). The normalized values for all the 8 representative features are provided in Supplementary Figure S3, available at http://links.lww.com/PAIN/B942. **Figure 2D** shows the common language effect size (see Methods section 2.6.5) for each feature relative to controls.

Compound pharmacology in DRG neurons is most simply evaluated based on firing frequency (total spikes/cell) and can be considered as 1-dimensional data—firing rates either increase or decrease. However, neuronal excitability arises from the interaction of many distinct ion channels and transporters that contribute to distinct aspects of the spike waveforms and timing. Many of these parameters show too much cell-to-cell variability to be useful in datasets comprising small numbers of neurons. All optical electrophysiology records from thousands of neurons, enabling reliable and robust analysis of parameters that reflect a richer picture of neuronal dynamics (eg, spike shape and timing at different stimulus intensities). This allows us to represent disease phenotypes and pharmacological responses in a multidimensional space, which can distinguish compounds that appear similar when the only output is firing frequency. Among all the compounds that can silence DRG neuron firing, we were primarily interested in compounds that restored the SPARC-induced phenotypes back to the nonsensitized naïve condition, in the multidimensional space represented by all the selected features.

Therefore, we quantified dose-dependent effects of compounds by 2 numbers: "phenotype score," a measure of phenotypic rescue that captures recovery along the vector between negative and positive controls, and "distance," a measure of total effects that incorporates both movement along the phenotypic axis and off-axis effects (**Fig. 2E**; Methods section 2.6.4 for details). A phenotype vector, p, was defined as the difference between the average SPARC-treated wells and the average no SPARC wells, in the absence of drug. A compound vector, c, was defined as the difference between wells treated with SPARC and drug (at a particular dose) and the average wells treated with SPARC only. The projection of the compound vector onto the phenotype vector was a measure of phenotypic rescue. We scaled this projection to create a "phenotype score," where 0 corresponded to perfect rescue and 1 corresponded to no rescue.

To measure compound effects orthogonal to p, we additionally calculated the Euclidean distance, d, between the compound plus SPARC well (orange dot in **Fig. 2E**) and the average no SPARC wells (purple dots in **Fig. 2E**) normalized to the phenotype vector length. This distance is a measurement of proximity between the SPARC-sensitized DRG neurons after compound treatment and the nonsensitized naïve DRG neurons in the 8-dimensional space based on 8 selected features. $d = 0$ corresponds to complete SPARC phenotype reversal with no orthogonal effects, whereas $d > 1$ indicates significant deviation from perfect phenotype reversal. For visualization purposes, we expressed p and c as 2-dimensional vectors by projection of the 8-dimensional phenotype space into its 2 leading principal components (**Fig. 2E**, Methods). **Figure 2F** shows example concentration–response trajectories. An ideal compound would reverse the SPARC phenotype (high efficacy) at low concentrations (high potency) with no orthogonal activity over this concentration range (**Fig. 2G**). Many compounds (eg, compound 1) showed a biphasic distance response, reflecting partial rescue of the SPARC phenotype at low concentrations, followed by "overcorrection" because of exaggerated pharmacology or off-target effects at higher concentrations (**Figs. 2F and G**). Note that an increase in d does not necessarily imply an increase in excitability.

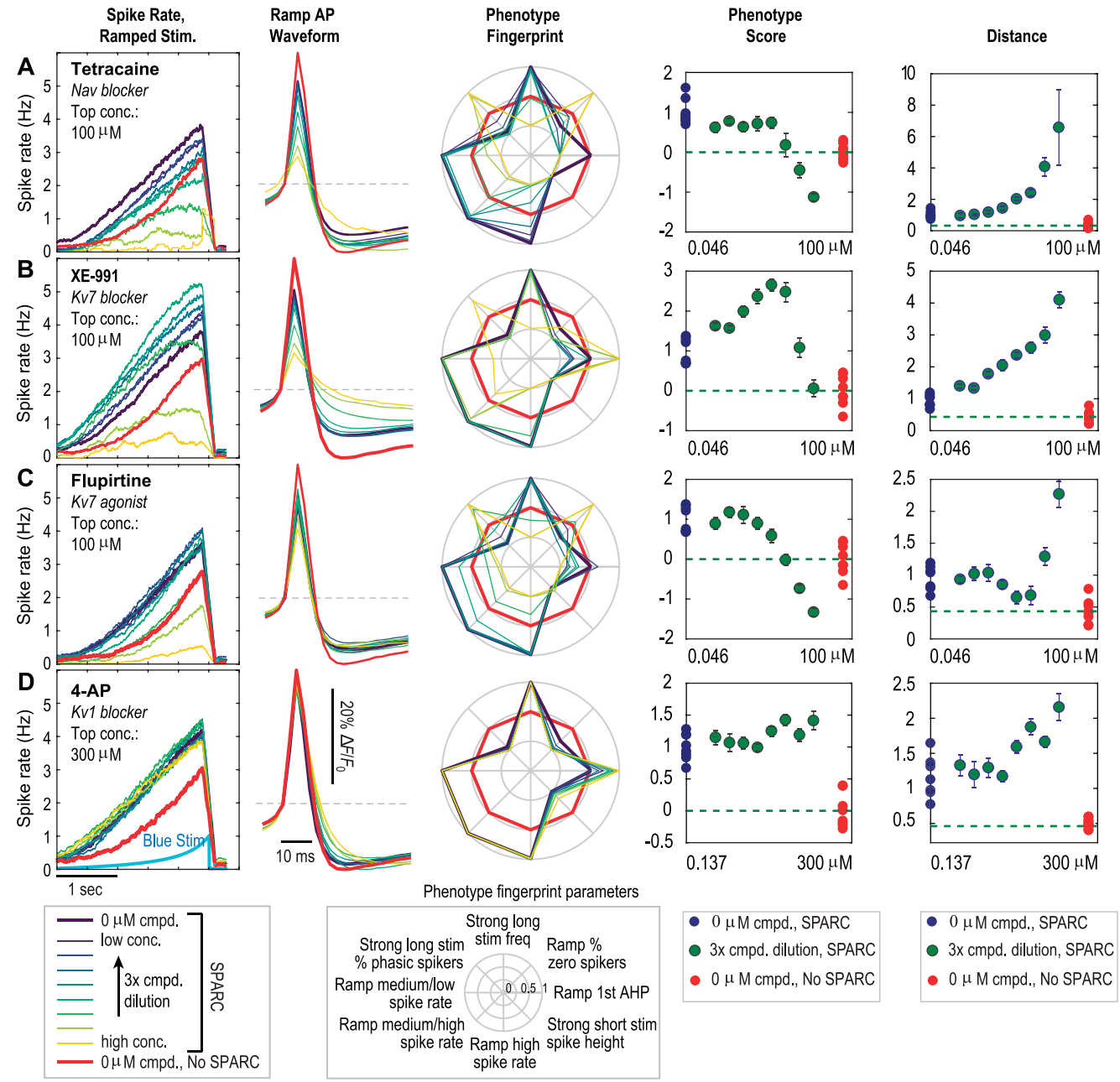

Figure 5. Compounds with distinct mechanisms of action showed differential phenotype reversal responses. Five plots are shown for each of the 4 compounds: spike rate (Hz) for ramp stimulus, AP waveform for ramp stimulus, phenotype radar plot, phenotype score, and distance score. Legend for experimental condition tested and radar plot parameters are listed at the bottom. (A) Tetracaine, an approved topical analgesic, is a nonselective, activity-dependent sodium channel blocker. It fully reversed the hyperexcitability phenotype at lower doses but perturbed the action potential waveform and firing at high concentrations. (B) XE-991, a Kv7 blocker, increased excitability at low doses and strongly perturbed both action potential waveform and firing rate at high doses. (C) Flupirtine, a Kv7 agonist, was formerly prescribed to treat pain in Europe. Flupirtine fully reversed the phenotype with mild effects on the action potential waveform. (D) 4-AP, a relatively nonselective Kv blocker, had mild effects on the spike rate and increased action potential width. The range of concentration, different for each compound and shown on x-axis, was selected so that published IC50 values lie in the center of the tested concentration range. AP, action potential; SPARC, sensitizing pain reagent composition.

3.4. Establishing an in vitro pain model of osteoarthritis using sensitized sensory neurons

We next extended the SPARC approach to model osteoarthritis pain. To this end, we developed OA-SPARC, a mixture of inflammatory mediators found in the synovial fluid of joints with chronic osteoarthritis pain[1–3,8,10,12,15,17,19–21,30,34,37,47,48,53,54,59,61,65,67–69,72,80,81,84,89,90,96–98,100,101,108,109,114] (**Fig. 3A**, **Table 1**). In patients, the first step in generation of these inflammatory mediators is physical joint damage, typically from age and/or obesity.[49,50] Resultant danger-associated molecular patterns, such as broken-down cartilage components and alarmins from damaged cells, are detected by local immune and repair cells. These cells in turn secrete inflammatory mediators, which accumulate in the synovial fluid, leak through the synovial membrane, and modulate sensory neuron firing. Compared with traditional inflammatory soup formulation with 4 ingredients (BK (Bradykinin), 5-HT, Histamine, and PGE2 (Prostaglandin E2)),[105] OA-SPARC has 9 ingredients in the formulation that meet the following criteria: (1) In humans, the mediator must be detected at increased levels in the synovial fluid of OA patient joints. (2) The associated receptor must be

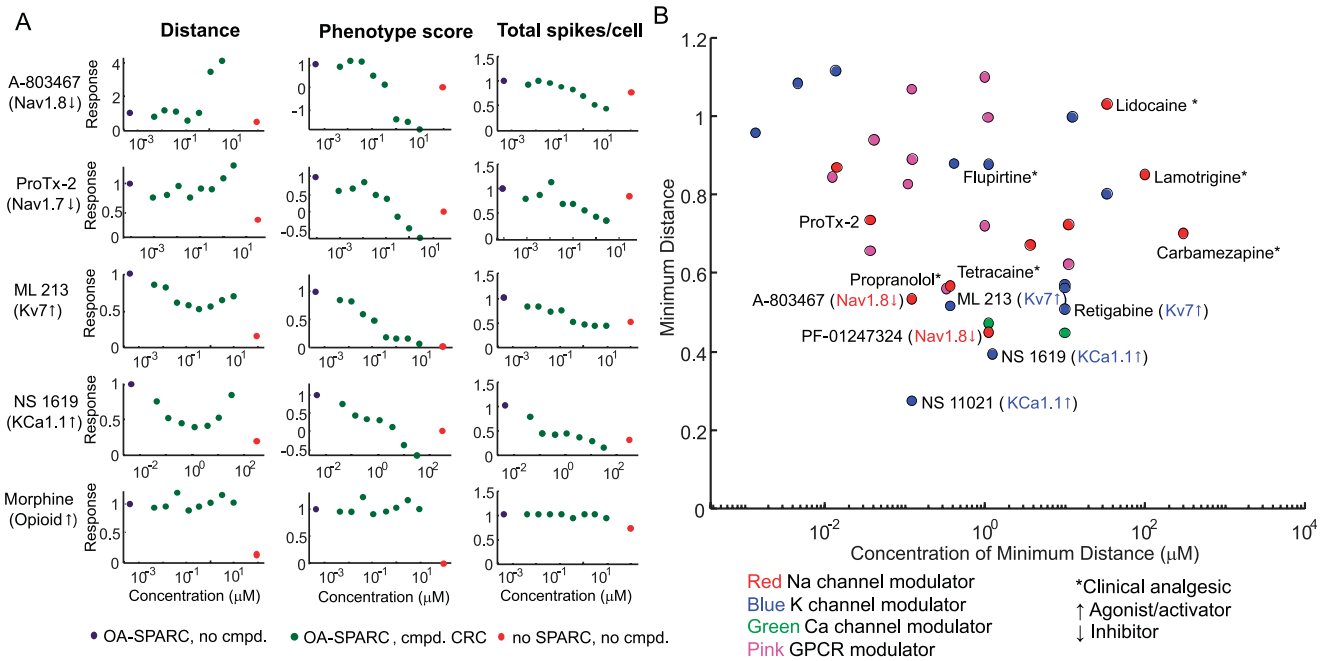

Figure 6. Analysis of diverse pharmacology in OA-SPARC model characterized performance characteristics of different compound mechanisms. (A) Concentration response curves for 5 compounds with diverse target mechanisms. Each panel shows an 8-point, 3× dilution series. The top concentration, different for each compound, was selected such that published IC50 values lie in the center of the tested concentration range. Each compound has 3 panels. The y-axis of the left panel indicates the distance between the compound well and the average no SPARC well as a measure of proximity between compound well and the naïve nonsensitized DRG wells, The y-axis of the middle panel indicates the phenotype score as a measure of compound effects on the phenotype rescue without consideration of compound unwanted side effects. The y-axis of the right panel indicates the average number of action potentials per DRG neuron elicited by the optogenetic stimulus protocol relative to the vehicle (no SPARC) wells. This excitability measure is reduced by many sodium channel inhibitors and potassium channel activators and increased by potassium channel inhibitors. (B) Minimum distance of 36 compounds with diverse target mechanisms are plotted vs the concentration at minimum distance, which is defined as the concentration at which the compound achieves maximal rescue effects on overall phenotypes. DRG, dorsal root ganglion; OA, osteoarthritis; SPARC, sensitizing pain reagent composition.

expressed in DRG neurons. (3) When applied to DRG neurons, the mediator must modify electrophysiology. (4) When injected in rodents, it must cause local pain. (5) After injection of the pain mediator, a pharmacological blocker of the associated receptor must alleviate pain in the injected rodent. (6) Ideally, a receptor agonist will enhance pain in the rodent. (7) Ideally, injection of the mediator will cause less pain in a mouse with receptor knockout. **Table 1** provides the formulation of OA-SPARC using these criteria.

Soluble factors mediate much of OA pain sensitization in vivo.[1,30,34,37,53,61,65,67,84,97,98,109] Approved therapeutics for OA pain have been developed targeting several components of OA-SPARC, including prostaglandin E2, nerve growth factor, and tumor necrosis factor alpha, supporting their roles in generation of OA pain.[5,7,26,28,41,87] However, the pleiotropic mechanisms in the complex OA-SPARC mixture suggest that a blocker of just one receptor activated by the SPARC will have limited therapeutic benefit. Thus, an OA-SPARC phenotypic screen is steered toward finding compounds that modulate overall excitability.

Cultured rat DRG neurons grow extensive neuronal processes (**Fig. 3B**) and express many of the key receptors for OA-SPARC sensitization roles in pain signaling (**Table 1**). When applied to cultured DRG neurons for 24 hours, OA-SPARC induced an ~3× increase in neuronal excitability (eg, frequency increased from 1.32 ± 0.03 Hz in no SPARC to 3.07 ± 0.07 Hz in OA-SPARC at the second long pulse with stimulus intensity at 58 mW/cm^2, mean ± SEM, $P < 0.001$) (**Figs. 3C and D**). We identified a subset of excitability parameters to summarize the OA-SPARC phenotype, including 6 spike timing features (firing frequency at strong long stim, % phasic spikers at strong long stim, % zero spikers at the ramp, spike rate at low, medium, or high end of the ramp) and 2 spike shape features (AHP depth at the first spike in the ramp, mean spike height at the strong short stim) (**Fig. 3E**; see Methods section 2.6.4 for detailed methods). The 8 parameters used to calculate the OA-SPARC phenotype overlap with but are not identical to the features used for the Inflam-SPARC phenotype.

In addition, we validated OA-SPARC in vivo with measurements of pain in rats (**Figs. 3F and G**). Osteoarthritis-sensitizing pain reagent composition was injected into the hind paw of rats and compared with vehicle and complete Freund adjuvant (CFA) controls. Pain was assayed by the von Frey test[120] (filament stiffness for first paw withdrawal) and the weight differential was applied to the 2 hind paws. Osteoarthritis-sensitizing pain reagent composition induced mechanical allodynia in paw withdrawal threshold, with effect size comparable with the CFA-positive control (eg, 72 hours after injection, paw withdrawal threshold was 12.7 ± 0.9 g in vehicle, 6.3 ± 0.4 g in CFA, 8.6 ± 0.7 g in 80× OA-SPARC, 7.5 ± 0.7 g in 400× OA-SPARC, and 7.3 ± 0.5 g in 2000× OA-SPARC, mean ± SD). Osteoarthritis-sensitizing pain reagent composition also induced statistically significant changes in weight-bearing measurements at short time points (eg, 8 hours after injection, weight-bearing difference between uninjected and injected paws changed from 5.0 ± 1.1 g to 7.0 ± 1.9 g in vehicle, 5.7 ± 0.5 g to 45.3 ± 1.5 g in CFA, 5.6 ± 0.7 g to 30.8 ± 0.5 g in 80× OA-SPARC, 5.7 ± 0.2 g to 33.6 ± 0.7 g in 400× OA-SPARC, and 5.6 ± 0.9 g to 34.8 ± 0.9 g in 2000× OA-SPARC, mean ± SD), indicating that OA-SPARC induced pain in vivo.

The final concentration for each of the OA-SPARC components was optimized, with each component titrated alone and in the

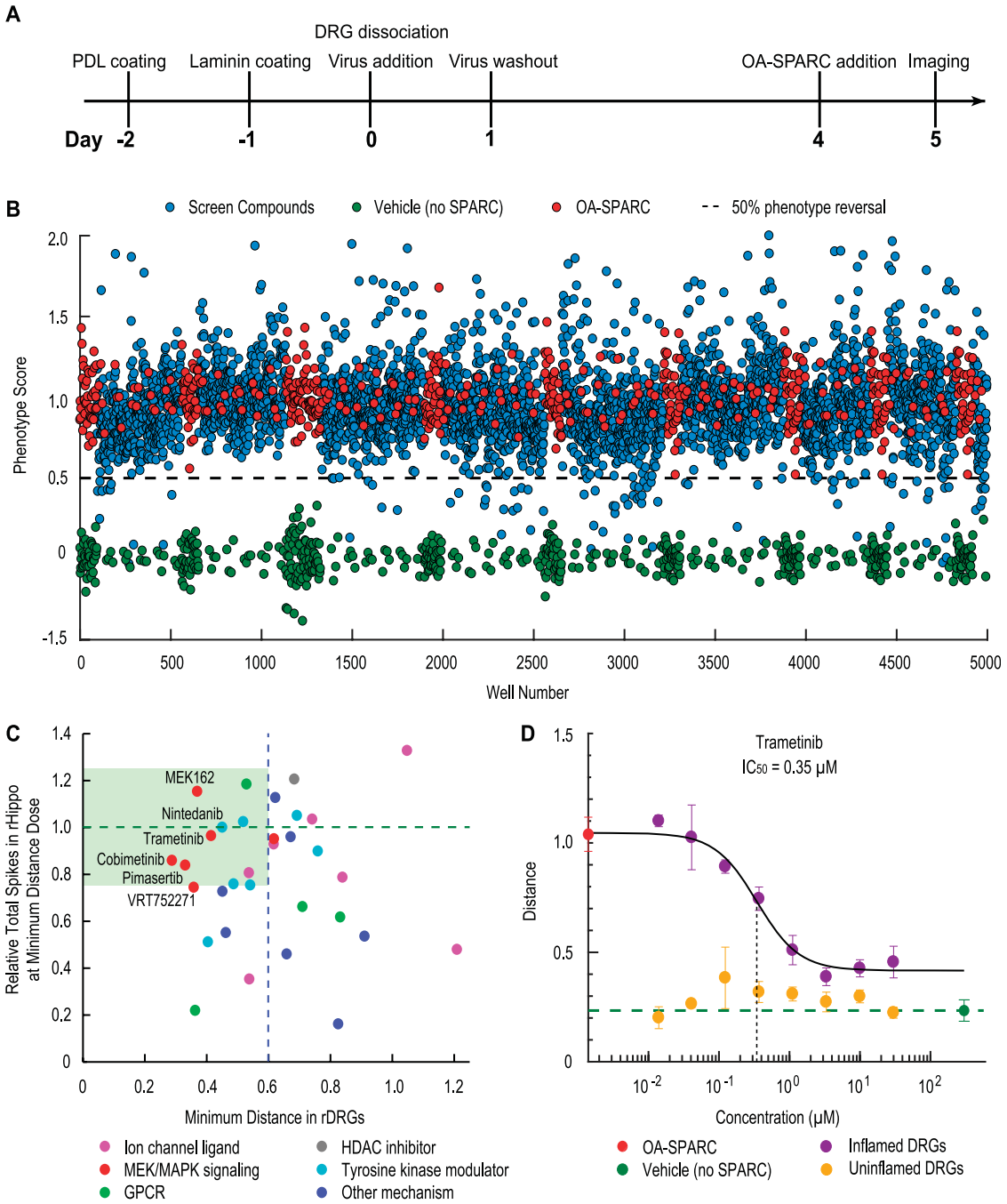

Figure 7. Phenotypic screen and hit validation identified known and novel mechanistic classes as potential analgesics. (A) Timeline for OA-SPARC assay. (B) Normalized phenotype score in pilot screen plates. Compounds were screened at 5 μM. Hit threshold is 0.5, indicating a 50% phenotype reversal. (C) Top ranked hits were validated using an 8-point, 3× dilution series in both OA-SPARC–sensitized DRG neurons and cultured rat hippocampal neurons. The x-axis indicates the minimum distance in OA-SPARC–sensitized DRG neurons (efficacy). The y-axis indicates the total spikes relative to the vehicle (no SPARC) wells in rat hippocampal neurons at the minimal distance dose. Blue dashed line indicates minimum distance of 0.6, ie, 40% phenotype reversal. Compounds within the green shaded area reversed more than 40% of the OA-SPARC phenotype with less than 25% perturbation of the spiking of hippocampal neurons, suggesting potential pain therapeutic mechanisms of interest. (D) Top ranked hits were validated using an 8-point, 3× dilutions series in both OA-SPARC–sensitized DRG neurons and uninflamed DRG neurons. Shown here is a top-ranked hit, Trametinib, that reversed the phenotype in a dose-dependent manner in OA-SPARC–sensitized DRG neurons but had little effect in uninflamed DRG neurons. DRG, dorsal root ganglion; HDAC, histone deacetylase inhibitor; MEK/MAPK, mitogen-activated protein kinase kinase/mitogen-activated protein kinase; OA, osteoarthritis; PDL, poly-d-lysine coating; SPARC, sensitizing pain reagent composition.

presence of the other components (**Fig. 4**). To confirm expression of the molecular targets of each of the 9 OA-SPARC components along with other critical DRG genes, we performed next-generation RNA sequencing (RNA-Seq) using uninflamed, cultured rat DRG neurons (see Methods section 2.7). We demonstrated expression of at least one molecular target for each ligand (**Table 1**) in the OA-SPARC. The RNA-Seq data confirmed a medium level of expression (1000 > TPM $\geq$ 11 for most of the OA-SPARC receptors in comparison with a set of reference genes [*Trpv1*, *Scn9a*, *Scn10a*, *Scn11a*]). Expression of receptors for CC motif chemokine ligand 2 was absent-to-low, which agreed with the small effect of this ligand when applied in isolation (**Fig. 4B**). The

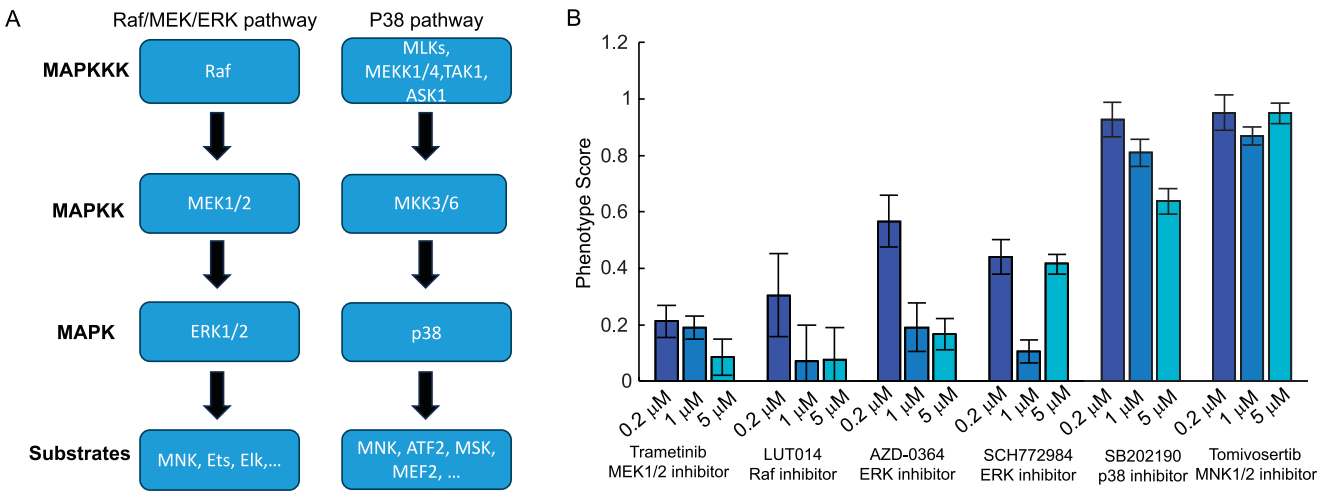

Figure 8. MAPK pathway tool compound pharmacology. (A) A diagram that illustrates the key targets in different MAPK pathways, including the Raf-MEK-ERK pathway and P38 pathway. (B) Tool compounds acting on different targets in Raf-MEK-ERK pathway or P38 pathway were tested at 3 different doses (0.2, 1, and 5 μM). Phenotype scores were plotted as mean ± SEM (n = 6 wells for each concentration). Phenotype score at zero means the compound can fully reverse the phenotypes to a state similar to no SPARC condition. All the tested tool compounds are potent kinase inhibitors with reported IC50 values <50 nM in the literature. SPARC, sensitizing pain reagent composition. MAPK, Mitogen-activated protein kinase; Raf/MEK/ERK pathway; extracellular signal-regulated kinase pathway involving Raf, MEK, and ERK enzymes.

combined effect of the full SPARC was much larger than for any individual ingredient, indicating that effects were additive or possibly synergistic. Removing any individual ingredient only modestly affected the hyperexcitability phenotype, suggesting redundancy in the hyperexcitability signaling pathways (**Fig. 4C**). Any compounds that fully reverse the SPARC-induced phenotype will likely operate by targeting nodes where signaling paths converge (**Fig. 4A**). The final optimized formulation maintained clinically observed concentrations, although we applied 10× OA-SPARC when screening to increase the signal window.

3.5. Sensory neuron osteoarthritis-sensitizing pain reagent composition excitability assay validation using control pharmacology

To build confidence in the translational value of the assay, we applied pharmacological agents with defined mechanisms of action (MOA), including known analgesics, to OA-SPARC-treated sensory neurons. We treated OA-SPARC–sensitized neurons with Na_V and K_V7 ion channel modulators, which are known to have strong effects on neuronal excitability. Cultured DRG neurons responded robustly to sodium and potassium channel modulators, and compound effects were broadly consistent with known MOAs. Tetracaine, a nonselective sodium channel blocker, reduced the hyperexcitability and phenotype score at low concentrations, but overcorrected the phenotype score, silenced cell firing, and displayed increased distance values at high concentrations (**Fig. 5A**). A K_V7 inhibitor (XE-991) did not reverse the OA-SPARC phenotype except at very high concentrations (**Fig. 5B**), whereas in contrast, flupirtine,[32] a K_V7-activating analgesic, reversed the hyperexcitability phenotype (**Fig. 5C**) and displayed both phenotype and distance score rescue, indicating reversal of the OA-SPARC phenotype at lower concentrations but overcorrection of the phenotype score and higher distance values at higher concentrations, indicating possible unwanted effects at high concentrations. A nonselective potassium channel inhibitor (4-AP) did not reverse the OA-SPARC phenotype (**Fig. 5D**). Clinically relevant analgesics tetracaine and flupirtine would be classified as active compounds in this assay, whereas the potassium channel blockers would not be selected as hits. These results demonstrated the ability of the all-optical electrophysiology in vitro models to identify and characterize compounds with in vivo analgesic activities.

To further examine the assay performance, we evaluated 36 compounds selected based on their diverse pharmacological profiles and clinical relevance for treating chronic pain (Supplementary Fig. S4, S5, S6, S7, available at http://links.lww.com/PAIN/B942). **Figure 6A** shows concentration response curves for 5 compounds that modulate ion channel and G protein-coupled receptor (GPCR) targets. Each compound has 3 associated panels, including distance, phenotype scores as in **Figure 5**, and the total number of APs fired per cell as a general measure of neuronal excitability, as a function of compound concentration. The assay was sensitive to a variety of mechanisms including nonselective sodium channel block, $Na_V1.7$ block, $Na_V1.8$ block, sodium channel activation, K_V7 activation, K_V7 inhibition, $K_{Ca}1.1$ activation, SK1 activation, K_V1 block, KCNK3/9/18 inhibition, and nociception opioid peptide (NOP) receptor agonism (**Fig. 6A**, Supplementary Fig. S4, S5, S6, S7, available at http://links.lww.com/PAIN/B942). As expected, potassium channel agonists and sodium channel blockers typically decreased excitability, whereas potassium channel inhibitors and sodium channel agonists increased excitability at low concentrations. For some compounds, such as K_V7 agonist ML-213,[122] both excitability and distance demonstrated compound efficacy and phenotype reversal. In contrast, K_V7 blockers increased distance and excitability measures (Supplementary Fig. S5, available at http://links.lww.com/PAIN/B942). In some cases, as for nonselective sodium channel blockers and A-803467 ($Na_V1.8$ blocker), the distance measures decreased at low concentration, then increased at higher doses, possibly indicating exaggerated pharmacology because of on-target effects or to engagement of additional targets at higher concentrations (**Fig. 6A**). Many clinical analgesics, indicated by a *, show reversal of SPARC-induced hyperexcitability over a portion of the dosing range.

Some clinical analgesics (Cox-2 inhibitor, opioid agonists) did not affect distance or excitability measures (Supplementary Fig. S7, available at http://links.lww.com/PAIN/B942), a consequence of low expression of the target or the target's minimal role in sensory neuron excitability. Distance measurements provided

insights that were not captured by simple excitability measures, as indicated by the divergence of distance and excitability measures at high concentrations for nonselective Na_V blockers. This divergence is an indicator of dose-limiting unwanted effects at high concentrations.

Therapeutic discovery efforts prioritize targets showing SPARC phenotype reversal at near-zero distances (ie, with little phenotypic effect orthogonal to the SPARC phenotype vector). Modulation of an ideal target would reverse the hyperexcitability phenotype with small distance (high efficacy) at low concentrations (high potency). **Figure 6B** plots the minimal distance of 36 compounds vs the concentration of minimal distance, which is defined as the concentration of a tested compound at which it maximally reduced the distance between the OA-SPARC–sensitized wells and nonsensitized DRG wells in the 8 parameter multidimensional space. Some clinically used analgesics, including carbamazepine, propranolol, and tetracaine, displayed clear activity with distance values in the 0.55 to 0.7 range. The $Na_V1.7$-blocking peptide ProTx-2 reversed the hyperexcitability phenotype at low concentrations, consistent with its role in pain transmission, but increased distance values at higher concentrations, possibly because of block of additional sodium channels at these concentrations. Eight compounds afforded a minimum distance <0.55. Surprisingly, 6 of the most active compounds fell into 3 MOAs: $Na_V1.8$ inhibitors (A-803467 and PF-01247324), K_V7 agonists (ML-213 and retigabine), and $K_{Ca}1.1$ agonists (NS 1619 and NS 11021). The concentration for these 6 compounds to achieve maximum rescue effects (concentration of minimum distance, A-803467: 0.123 μM; PF-012347324, 1.11 μM; ML-213, 0.37 μM; retigabine, 10 μM; NS 1619, 1.23 μM; NS 11021, 0.123 μM) are all within 6-fold of their reported IC50/EC50 values (A-803467: 0.14 μM[45]; PF-012347324, 0.45 μM[83]; ML-213, 0.23 μM[121]; retigabine, 1.9 μM[104]; NS 1619, 3 μM[44]; NS 11021, 0.4 μM[44]), suggesting Nav1.8, K_V7 and $K_{Ca}1.1$ channels as potential analgesic targets for OA pain, consistent with literature evidence.[29,40,74,82,85,91,125] The fact that each target was confirmed by 2 different compounds highlights the robust ability of the assay to identify candidate targets. Several other Na_V channel inhibitors and known analgesics fell between 0.5 and 0.8 distance score. Interestingly, Ca_V1 agonist Bay K8644 and Ca_V2 inhibitor ziconotide also seem to be effective in this analysis (Supplementary Fig. S6, available at http://links.lww.com/PAIN/B942). However, the concentrations for Bay K8644 and ziconotide to achieve maximum rescue effects (concentration of minimum distance: 1.1 μM for Bay K8644 and 10 μM for ziconotide) were much higher than their reported IC50/EC50 values (17 nM for Bay K8644[86] and 72 nM for ziconotide[94]), which suggests observed effects may have off-target contributions.

3.6. Optimization of osteoarthritis-sensitizing pain reagent composition excitability assay for screening applications

We then sought to optimize the assay for high-throughput screening by improving the yield of active neurons and increasing the screening window. Experimental parameters that were optimized include plate type and coating protocol, OA-SPARC preparation and storage protocol, DRG dissociation protocol, plating and culture media, neurotrophic factors, cell density, viral doses, optogenetic construct promoter, imaging temperature, imaging scan pattern, imaging buffer composition, and optogenetic stimulus protocol. Final conditions are described in the Methods section. Rat DRG neuronal preparations were plated and treated with lentiviral particles encoding all-optical physiology components on day 0 and imaged 5 to 8 days later (**Fig. 7A**). With 3 dissections per week, we screened 1440 compounds/week. The optimized assay also had minimal time-on-microscope and plate edge effects. A full sentinel plate with zebra layout of "SPARC" and "no SPARC" wells was included in each dissection round to assess Z′ values of the OA-SPARC phenotype.

We evaluated DMSO tolerance to identify DMSO levels that produce <10% changes in the assay window compared with buffer control. We found that 0.5% DMSO was tolerated for 48 hours, although we proceeded with 0.1% DMSO for screening. We confirmed assay stability using 3 consecutive rounds of experiments. The assay achieved a stable Z' > 0.3, which is sufficient for screening: assuming well scores follow Gaussian distributions and optimal thresholding, an assay with Z' = 0.3 has a theoretical 77% chance of 0 false positives or negatives in a 14,000-compound screen. We also tested assay stability using IC_{50} values of 2 control compounds, tetracaine (Na_V blocker) and ML-213 (K_V7 agonist). In 3 rounds of measurements, tetracaine and ML-213 were assayed in 8-pt concentration-response curve (CRC) experiments in quadruplicate. IC_{50} values of both compounds varied <3× across 3 rounds (tetracaine: 2.5, 6.6, and 5.3 μM; ML-213: 0.51, 0.68, and 0.71 μM), confirming assay stability. The optimal screening concentration was selected by testing 2 screening plates randomly selected from an internal master library of ~200,000 CNS-focused, commercially available small-molecule compounds. These plates were screened at 1, 3, and 5 μM with 0.1% DMSO concentration. To rank compounds in high-throughput screening, we used the phenotype score, defined above (**Fig. 2**). In subsequent compound profiling in CRC experiments, we used the distance measure, *d*, to probe orthogonal effects as described in **Figure 2**. We selected phenotype score = 0.5 as the hit threshold corresponding to a 50% phenotype reversal and 5 μM as the compound concentration for screening, which maximized total number of active neurons and minimized total side effects summed over all hits.

3.7. Phenotypic screen of annotated library

We screened approved drug and mechanistically focused libraries, including a library of ~2400 approved drugs (FDA, EMA, and other agencies) assembled from 4 commercial libraries (Prestwick, Enzo, ApexBio, and TargetMol) and a series of annotated libraries from Biomol targeting diverse neuronal proteins containing 842 additional compounds that are known to interact with neuronal signaling and regulatory mechanisms. **Figure 7B** shows overall assay performance with an average Z' = 0.42 for all plates in the screen. Using the hit threshold we established during the optimization phase, we identified 133 hits including 109 antagonists that reversed the phenotype with minimal side effect scores and 24 agonists that significantly exacerbated the phenotype. The 4.4% hit rate is in line with expectations as the libraries are composed of pharmacologically active compounds. The phenotype reversal scores for all the screened compounds are provided as a supplementary file (OA-SPARC primary screen results.xlsx, available at http://links.lww.com/PAIN/B941).

The 133 hits from the screen were retested in duplicate at the screening concentration (5 μM) and at 1 μM. The hit confirmation rate was calculated as the fraction of compounds for which the mean of the duplicate retest measurements at 5 μM separated from control wells by at least 3 SD.[33] Of the 109 antagonists selected in the screen, 45 compounds (41%) were confirmed. Of the 24 agonists selected in pilot screen, 19 compounds (79%) were confirmed. The overall hit confirmation rate was 48% (64 of 133 compounds).

The 33 top-ranked and confirmed antagonist hits (Supplementary table 1, available at http://links.lww.com/PAIN/B942) that were commercially available were reordered as fresh samples from alternative vendors when possible and were then counter-screened in 2 additional optical electrophysiology assays to identify potential off-target effects in the central nervous system (CNS) and in unsensitized DRG neurons. To detect undesired activity in the CNS, we counter-screened the 33 hits in 8-point CRC in cultured rat hippocampal neurons, using an optical excitability assay (Methods section). **Figure 7C** compares the efficacy in the OA-SPARC DRG assay (x-axis) vs CNS effects (y-axis). Ideal compounds reside in the shaded region and show clear OA-SPARC phenotype reversal (low minimal distance values) with minimal effects on AP frequency in hippocampal neurons. Concentration–response curve results provide a means to rank hits, to evaluate assay reliability and hit criteria and to validate whether hits impacted excitability via an OA-SPARC–related mechanism.

We then counter-screened the 15 antagonists that showed minimal CNS perturbation in un-inflamed DRG neurons, to assess specific reversal of the OA-SPARC phenotype and to search for compounds with minimal effects on normal sensory activity. Trametinib, a MEK inhibitor, showed no effect on the parameters used to define the OA-SPARC phenotype in DRG sensory neurons without OA-SPARC sensitization (**Fig. 7D**), indicating a selective effect on OA-SPARC–induced hyperexcitability.

A detailed analysis of the confirmed hits revealed several common molecular pathways (eg, sodium channel inhibitors) and candidate analgesia targets. Interestingly, 6 mitogen-activated protein kinase (MEK) inhibitors were confirmed as reversing the OA-SPARC phenotype, consistent with previous findings that intrathecal administration of the selective MEK inhibitor PD 198306 dose-dependently blocked static allodynia in both the streptozocin and the chronic constriction injury (CCI) models of neuropathic pain.[22,64] Trametinib, a MEK inhibitor, showed >70% reversal of the OA-SPARC phenotype with an EC_{50} value of ~350 nM (**Fig. 7D**). MEK is reported to be a key player downstream of multiple pain-related signaling pathways, including TNFα (tumor necrosis factor alpha), NGF (nerve growth factor), IL-6 (Interlukin-6), and PGE2 (Prostaglandin E2).[52,58,63,112,113,119] MEK activation has also been reported to increase DRG neuron excitability via modulation of multiple ion channels. For example, TNFα treatment can induce DRG hyperexcitability via MAPK activation–dependent changes in gating of Nav1.8 and Nav1.9[38]; NGF treatment can increase DRG excitability via ERK1/2 (a downstream target of MEK1/2) activation, which can phosphorylate and alter gating properties of Nav1.7.[103] Our identification of MEK as a target supports the hypothesis that compounds acting on convergent points of multiple pathways are more likely to demonstrate greater phenotype reversal.

MEK represents an important class of targets in MAPK pathways, and different MAPK pathways are involved in diverse cellular physiological functions.[92,124] To further explore MEK signaling, we tested tool compounds inhibiting the Raf/MEK/ERK signaling cascade and in an analogous MAPK cascade involving P38 (**Fig. 8A**). We also tested an inhibitor of MNK, which is a downstream target of MAPK pathways implicated in the development of neuropathic pain.[99] Our results suggest that compounds inhibiting Raf, MEK, and ERK substantially reversed the OA-SPARC–induced phenotype in a dose-dependent manner (**Fig. 8B**). p38 inhibition reversed the phenotype to a much lower degree, and MNK inhibition showed minimal phenotype reversal (**Fig. 8B**). These results imply that the Raf/MEK/ERK signaling plays an important role in integrating upstream signals triggered by OA-SPARC and highlights the utility of our approach in dissecting pain signaling pathways.

Two histone deacetylase inhibitors were also confirmed, consistent with their interference role in the epigenetic process of histone acetylation and analgesic properties in models of chronic inflammatory pain.[25,62]

Finally, 19 agonists that enhanced the OA-SPARC phenotype were evaluated in CRC to investigate potential mechanisms associated with pain signaling pathways and to identify potential adverse effects of approved drugs. Supplementary Fig. S8A, available at http://links.lww.com/PAIN/B942, presents a list of the 9 top-ranked agonist hits. These compounds may provide insight into potential pathways involved in generating a proalgesic condition and as a signal of potential off target effects of known drugs. For example, chemotherapeutics cisplatin and carboplatin are well known to induce peripheral neuropathy in some patients.[16,106] Supplementary Fig. S8B, available at http://links.lww.com/PAIN/B942, presents the CRC data for 4 agonists tested in the absence and presence of OA-SPARC. All 4 compounds were active in both the absence and the presence of OA-SPARC. The concentrations for half maximal effects in the DRG assay for some compounds were within clinically relevant ranges of in vivo exposure. In some cases, the agonist effects on DRG activity may not be coupled to the primary pharmacological mechanism; loratadine is a widely used antihistamine (H1 receptor antagonist), which also blocks KCNK18, a potassium channel involved in pain.[13] Further exploration of these hits may yield new information on pathways involved in generating or reducing hypersensitivity in sensory neurons for OA pain.

4. Discussion

Over recent decades, the pharmaceutical industry has focused predominantly on target-based approaches to develop new pain therapeutics because associated high-throughput methods enable efficient screening of large libraries and rapid characterization of analogues.[14,118] Additionally, knowing the target aids rational molecular design during medicinal chemistry optimization, helps guide preclinical safety studies, and enables development of target engagement strategies in clinical trials. Despite these advantages, the scarcity of new classes of analgesic drugs argues for establishing alternative development pipelines, including phenotypic screening.[46]

Phenotypic assays historically played an important role in pain drug discovery. The widely used pain therapeutics gabapentin (Neurotin) and pregabalin (Lyrica) were initially discovered as anticonvulsant agents using phenotypic screens before identification of the $\alpha_2\delta$-$_1$ subunit of voltage-gated calcium channels as the molecular target.[31] Proven success of phenotypic approaches is leading to a resurgence in use for some therapeutic areas.[27,110,126] Because compounds are screened in a disease-relevant cellular system, measured responses can be more predictive of clinical results. Compounds that strongly modulate sensory neuronal function in vitro are likely to modulate function of the same neurons in vivo. For example, cultured neurons can contain appropriate protein splice isoforms, expression levels, posttranslational modifications, and interacting partners, which can dramatically affect drug performance.

Phenotypic screening also casts a broad net: there are over 12,000 mRNA transcripts expressed in the human DRG, >3000 of which are elevated relative to fibroblasts or Schwann cells.[88] One hundred forty-one protein-coding genes are expressed at elevated levels relative to central nervous system (CNS) tissue[88]

and so are potential drug targets with lower risk for on-target toxicity. A phenotypic screen will be sensitive to modulation of many of the targets and can detect pleiotropic drugs,[70] which have the potential for greater efficacy than a single-target compound because of synergistic effects. By using a primary phenotypic screen in DRG neurons and phenotypic counter screens in CNS neurons and cardiomyocytes, the approach will also be sensitive to safety issues arising from pleiotropic effects. An example pleiotropic drug is clozapine, a highly efficacious atypical antipsychotic that interacts with multiple receptors.[79] Combining the phenotypic screening approach described in this study with post hoc immunohistochemical analysis may make it possible to perform a phenotypic screen on specific sensory neuron subtypes.

Identification of multiple compounds acting on the same target or the same signaling pathway in a phenotypic screen can point to new targets or pathways for drug discovery investigations. Our data suggests that the Raf/MEK/ERK pathway may be important for OA-SPARC–mediated DRG sensitization. MAPK pathway activation is a well-known mechanism related to OA disease progression and can lead to cartilage destruction in the joints of patients with OA and pain induction.[56] Our data suggest that the MAPK pathway, particularly the Raf/MEK/ERK axis, may play additional roles related to OA disease pathology based on sensitization of sensory neurons. MAPK inhibitors may offer therapeutic benefits for patients with OA because of their dual mechanism in reducing cartilage destruction and reversing DRG hyperexcitability. However, safety concerns of currently available MAPK inhibitors limit the application of these compounds to severe disease indications (eg, cancer).[56] Additional efforts are needed to discover isoform-specific MAPK inhibitors with improved safety profiles, which may be feasible for OA treatment.[56]

The probability of success for a phenotypic screen depends on the translatability of the assay to clinical outcomes, both the cellular model and the assay readout. Our cellular "pain-in-a-dish" model for OA pain induced rat DRG neuronal sensitization via OA-SPARC, a novel formulation of inflammatory mediators present at elevated levels in arthritic joints. Osteoarthritis-sensitizing pain reagent composition application drove a strong in vitro hyperexcitability phenotype in the cultured DRG neurons and caused pain in vivo when injected into a rat paw. The use of a rodent DRG model is supported by the fact that 128 of the 141 protein-coding genes that are expressed at elevated levels in DRG relative to central nervous system (CNS) in humans have conserved orthologs in mice.[88] Human induced pluripotent stem cell–derived sensory neurons are emerging as tools for pain disorder modeling induced by genetic mutations[71,76] but so far have limited applications in modeling pain induced by inflammatory mediators, including OA. To build confidence in the primary rat neuronal model, we pharmacologically validated the model by showing hyperexcitability reversal with clinical analgesics and sensible responses to a battery of potent and selective compounds with diverse targets.

The OA-SPARC model has been enabled for drug discovery by pairing with a high-throughput all-optical electrophysiology platform.[117] Manual patch clamp electrophysiology provides exquisite sensitivity but at the expense of throughput. Automated patch clamp studies provide detailed compound mechanisms but are limited by high cost, modest throughput and do not work well in intact cultured neurons. Calcium imaging provides high throughput by leveraging optical methods but lacks targeted stimulation and temporal resolution required to detect action potentials. Similarly, fluorescence plate readers provide high throughput but are associated with low temporal and spatial resolution and thus provide limited mechanistic information. The resulting translational challenge for pain drug discovery and for CNS-based disorders more broadly is significant, necessitating new approaches to bridge this important gap.

The combination of enabling screening technology and pain-relevant in vitro models provides promising opportunities for identification of improved therapeutics and exploration of pain signaling pathways. Because this platform is compatible with primary DRG neurons from different species, it is feasible to validate the key discoveries made in rodents using nonhuman primate and human primary DRG neurons. Recent progress in development of induced pluripotent stem cell–derived sensory neurons[24] can provide an avenue to large-scale generation of relevant human cell types to enable high throughput phenotypic screening for pain therapeutics to additionally provide a scalable means to evaluate and rank compounds for sensory cell activity as part of target-based pain therapeutic development projects. Finally, we anticipate that other forms of chronic pain induced by defined mixtures of inflammatory mediators, such as those secreted by tumors in cancer pain, may be modeled by taking a similar approach as the one described in this study.

Conflict of interest statement

P.W.L., H.Z., C.A.W., M.P., S.J.R., C.L.L., J.J., J.G., J.F., G.L., D.Z., N.B., A.B., R.C., A.E.E., L.A.W., G.T.D., and O.B.M. are current or former employees of Q-State Biosciences, now Quiver Bioscience, and may hold stock options. A.E.C. is on the scientific advisory board of Quiver Bioscience..

Acknowledgements

The authors thank Ted Brookings and Trinh Nguyen for early contributions to assay establishment and analysis tools. This work was funded in part by NIH grant 5R44AR074820.

Supplemental digital content

Supplemental digital content associated with this article can be found online at http://links.lww.com/PAIN/B942 and http://links.lww.com/PAIN/B941.

Article history:
Received 16 December 2022
Received in revised form 24 August 2023
Accepted 30 August 2023
Available online 14 November 2023

References

[1] Andratsch M, Mair N, Constantin CE, Scherbakov N, Benetti C, Quarta S, Vogl C, Sailer CA, Uceyler N, Brockhaus J, Martini R, Sommer C, Ulrich Zeilhofer H, Muller W, Kuner R, Davis JB, Rose-John S, Kress M. A key role for gp130 expressed on peripheral sensory nerves in pathological pain. J Neurosci 2009;29:13473–83.
[2] Andreev NY, Dimitrieva N, Koltzenburg M, McMahon SB. Peripheral administration of nerve growth factor in the adult rat produces a thermal hyperalgesia that requires the presence of sympathetic post-ganglionic neurones. PAIN 1995;63:109–15.
[3] Arnalich F, de Miguel E, Perez-Ayala C, Martinez M, Vazquez JJ, Gijon-Banos J, Hernanz A. Neuropeptides and interleukin-6 in human joint inflammation. Relationship between intraarticular substance P and interleukin-6 concentrations. Neurosci Lett 1994;170:251–4.
[4] Barabas ME, Kossyreva EA, Stucky CL. TRPA1 is functionally expressed primarily by IB4-binding, non-peptidergic mouse and rat sensory neurons. PLoS One 2012;7:e47988.

[5] Basbaum AI, Bautista DM, Scherrer G, Julius D. Cellular and molecular mechanisms of pain. Cell 2009;139:267–84.
[6] Bates D, Mächler M, Bolker B, Walker S. Fitting linear mixed-effects models using lme4. Journal of Statistical Software 2015;67:1–48.
[7] Bazan NG, Flower RJ. Lipid signals in pain control. Nature 2002 420: 135–8.
[8] Bellucci F, Meini S, Cucchi P, Catalani C, Nizzardo A, Riva A, Guidelli GM, Ferrata P, Fioravanti A, Maggi CA. Synovial fluid levels of bradykinin correlate with biochemical markers for cartilage degradation and inflammation in knee osteoarthritis. Osteoarthritis Cartilage 2013;21: 1774–80.
[9] Benjamini Y, Hochberg Y. Controlling the false discovery rate: a practical and powerful approach to multiple testing. J R Stat Soc Ser B (Methodological) 1995;57:289–300.
[10] Binshtok AM, Wang H, Zimmermann K, Amaya F, Vardeh D, Shi L, Brenner GJ, Ji R-R, Bean BP, Woolf CJ, Samad TA. Nociceptors are interleukin-1beta sensors. J Neurosci 2008;28:14062–73.
[11] Borja GB, Shroff H, Upadhyay H, Liu PW, Baru V, Cheng Y-C, McManus OB, Williams LA, Dempsey GT, Werley CA. Probing synaptic signaling with optogenetic stimulation and genetically encoded calcium reporters. Methods Mol Biol 2021;2191:109–34.
[12] Brenneman DE, Eiden LE. Vasoactive intestinal peptide and electrical activity influence neuronal survival. Proc Natl Acad Sci U S A 1986;83: 1159–62.
[13] Bruner JK, Zou B, Zhang H, Zhang Y, Schmidt K, Li M. Identification of novel small molecule modulators of K2P18.1 two-pore potassium channel. Eur J Pharmacol 2014;740:603–10.
[14] Burgess G, Williams D. The discovery and development of analgesics: new mechanisms, new modalities. J Clin Invest 2010;120:3753–9.
[15] Burgess GM, Mullaney I, McNeill M, Dunn PM, Rang HP. Second messengers involved in the mechanism of action of bradykinin in sensory neurons in culture. J Neurosci 1989;9:3314–25.
[16] Calls A, Torres-Espin A, Navarro X, Yuste V, Udina E, Bruna J. Cisplatin-induced peripheral neuropathy is associated with neuronal senescence-like response. Neuro Oncol 2021;23:88–99.
[17] Cesare P, McNaughton P. A novel heat-activated current in nociceptive neurons and its sensitization by bradykinin. Proc Natl Acad Sci U S A 1996;93:15435–9.
[18] Chandra MP. On the generalised distance in statistics. Proc Natl Inst Sci Ind 1936;2:49–55.
[19] Chaudhary P, Baumann TK. Expression of VPAC2 receptor and PAC1 receptor splice variants in the trigeminal ganglion of the adult rat. Mol Brain Res 2002;104:137–42.
[20] Chen S, Zhou Y, Li J, Shan LQ, Fan QY. The effect of bradykinin B2 receptor polymorphisms on the susceptibility and severity of osteoarthritis in a Chinese cohort. J Biomed Biotechnol 2012;2012:597637.
[21] Chuang HH, Prescott ED, Kong H, Shields S, Jordt SE, Basbaum AI, Chao MV, Julius D. Bradykinin and nerve growth factor release the capsaicin receptor from PtdIns(4,5)P2-mediated inhibition. Nature 2001;411:957–62.
[22] Ciruela A, Dixon A, Bramwell S, Gonzalez M, Pinnock R, Lee K. Identification of MEK1 as a novel target for the treatment of neuropathic pain. Br J Pharmacol 2003;138:751–6.
[23] Connor AB. Neuropathic pain: quality-of-life impact, costs and cost effectiveness of therapy. Pharmacoeconomics 2009;27:95–112.
[24] Deng T, Jovanovic VM, Tristan CA, Weber C, Chu P-H, Inman J, Ryu S, Jethmalani Y, Ferreira de Sousa J, Ormanoglu P, Twumasi P, Sen C, Shim J, Jayakar S, Bear Zhang HX, Jo S, Yu W, Voss TC, Simeonov A, Bean BP, Woolf CJ, Singeç I. Scalable generation of sensory neurons from human pluripotent stem cells. Stem Cell Rep 2023;18:1030–47.
[25] Denk F, Huang W, Sidders B, Bithell A, Crow M, Grist J, Sharma S, Ziemek D, Rice A, Buckley N, McMahon S. HDAC inhibitors attenuate the development of hypersensitivity in models of neuropathic pain. PAIN 2013;154:1668–79.
[26] Denk F, Bennett DL, McMahon SB. Nerve growth factor and pain mechanisms. Annu Rev Neurosci 2017;40:307–25.
[27] Eder J, Sedrani R, Wiesmann C. The discovery of first-in-class drugs: origins and evolution. Nat Rev Drug Discov 2014;13:577–87.
[28] Eitner A, Hofmann GO, Schaible HG. Mechanisms of osteoarthritic pain. Studies in humans and experimental models. Front Mol Neurosci 2017; 10:349.
[29] Faber CG, Lauria G, Merkies ISJ, Cheng X, Han C, Ahn H-S, Persson A-K, Hoeijmakers JGJ, Gerrits MM, Pierro T, Lombardi R, Kapetis D, Dib-Hajj SD, Waxman SG. Gain-of-function Nav1.8 mutations in painful neuropathy. Proc Natl Acad Sci 2012;109:19444–9.
[30] Ferreira J, Beirith A, Mori MAS, Araújo RC, Bader M, Pesquero JB, Calixto JB. Reduced nerve injury-induced neuropathic pain in kinin B1 receptor knock-out mice. J Neurosci 2005;25:2405–12.
[31] Field MJ, Cox PJ, Stott E, Melrose H, Offord J, Su T, Bramwell S, Corradini L, England S, Winks J, Kinloch RA, Hendrich J, Dolphin AC, Webb T, Williams D. Identification of the α_2-δ-1 subunit of voltage-dependent calcium channels as a molecular target for pain mediating the analgesic actions of pregabalin. Proc Natl Acad Sci 2006;103:17537–42.
[32] Fleckenstein J, Sittl R, Averbeck B, Lang PM, Irnich D, Carr RW. Activation of axonal Kv7 channels in human peripheral nerve by flupirtine but not placebo—therapeutic potential for peripheral neuropathies: results of a randomised controlled trial. J Translat Med 2013;11:34.
[33] Fogel P, Collette P, Dupront A, Garyantes T, Guédini D. The confirmation rate of primary hits: a predictive model. J Biomol Screen 2002;7:175–90.
[34] Fukuoka H, Kawatani M, Hisamitsu T, Takeshige C. Cutaneous hyperalgesia induced by peripheral injection of interleukin-1β in the rat. Brain Res 1994;657:133–40.
[35] Gereau RW, Sluka KA, Maixner W, Savage SR, Price TJ, Murinson BB, Sullivan MD, Fillingim RB. A pain research agenda for the 21st century. J Pain 2014;15:1203–14.
[36] Grosser T, Woolf CJ, FitzGerald GA. Time for nonaddictive relief of pain. Science 2017;355:1026–7.
[37] Grunke M, Schulze-Koops H. Successful treatment of inflammatory knee osteoarthritis with tumour necrosis factor blockade. Ann Rheum Dis 2006;65:555–6.
[38] Gudes S, Barkai O, Caspi Y, Katz B, Lev S, Binshtok AM. The role of slow and persistent TTX-resistant sodium currents in acute tumor necrosis factor-α-mediated increase in nociceptors excitability. J Neurophysiol 2015;113:601–19.
[39] Haanpää ML, Gourlay GK, Kent JL, Miaskowski C, Raja SN, Schmader KE, Wells CD. Treatment considerations for patients with neuropathic pain and other medical comorbidities. Mayo Clin Proc 2010;85:S15–25.
[40] Hameed S. Nav1.7 and Nav1.8: role in the pathophysiology of pain. Mol Pain 2019;15:174480691985880.
[41] Hefti FF, Rosenthal A, Walicke PA, Wyatt S, Vergara G, Shelton DL, Davies AM. Novel class of pain drugs based on antagonism of NGF. Trends Pharmacol Sci 2006;27:85–91.
[42] Helmick CG, Felson DT, Lawrence RC, Gabriel S, Hirsch R, Kwoh CK, Liang MH, Kremers HM, Mayes MD, Merkel PA, Pillemer SR, Reveille JD, Stone JH. Estimates of the prevalence of arthritis and other rheumatic conditions in the United States. Part I. Arthritis Rheum 2008; 58:15–25.
[43] Hochbaum DR, Zhao Y, Farhi SL, Klapoetke N, Werley CA, Kapoor V, Zou P, Kralj JM, Maclaurin D, Smedemark-Margulies N, Saulnier JL, Boulting GL, Straub C, Cho YK, Melkonian M, Wong GK-S, Harrison DJ, Murthy VN, Sabatini BL, Boyden ES, Campbell RE, Cohen AE. All-optical electrophysiology in mammalian neurons using engineered microbial rhodopsins. Nat Methods 2014;11:825–33.
[44] Honrath B, Krabbendam IE, Culmsee C, Dolga AM. Small conductance Ca2+-activated K+ channels in the plasma membrane, mitochondria and the ER: pharmacology and implications in neuronal diseases. Neurochem Int 2017;109:13–23.
[45] Jarvis MF, Honore P, Shieh C-C, Chapman M, Joshi S, Zhang X-F, Kort M, Carroll W, Marron B, Atkinson R, Thomas J, Liu D, Krambis M, Liu YY, McGaraughty S, Chu K, Roeloffs R, Zhong C, Mikusa JP, Hernandez G, Gauvin D, Wade C, Zhu C, Pai M, Scanio M, Shi L, Drizin I, Gregg R, Matulenko M, Hakeem A, Gross M, Johnson M, Marsh K, Wagoner PK, Sullivan JP, Faltynek CR, Krafte DS. A-803467, a potent and selective Nav1.8 sodium channel blocker, attenuates neuropathic and inflammatory pain in the rat. Proc Natl Acad Sci 2007;104:8520–5.
[46] Jayakar S, Shim J, Jo S, Bean BP, Singeç I, Woolf CJ. Developing nociceptor-selective treatments for acute and chronic pain. Sci Transl Med 2021;13:eabj9837.
[47] Jin X, Gereau RW. Acute p38-mediated modulation of tetrodotoxin-resistant sodium channels in mouse sensory neurons by tumor necrosis factor-α. J Neurosci 2006;26:246–55.
[48] Jung H, Toth PT, White FA, Miller RJ. Monocyte chemoattractant protein-1 functions as a neuromodulator in dorsal root ganglia neurons. J Neurochem 2008;104:254–63.
[49] Katz JN, Arant KR, Loeser RF. Diagnosis and treatment of hip and knee osteoarthritis: a review. JAMA 2021;325:568–78.
[50] King LK, March L, Anandacoomarasamy A. Obesity & osteoarthritis. Indian J Med Res 2013;138:185–93.
[51] Kiskinis E, Kralj JM, Zou P, Weinstein EN, Zhang H, Tsioras K, Wiskow O, Ortega JA, Eggan K, Cohen AE. All-optical electrophysiology for high-throughput functional characterization of a human iPSC-derived motor neuron model of ALS. Stem Cell Rep 2018;10:1991–2004.
[52] Kitanaka T, Nakano R, Kitanaka N, Kimura T, Okabayashi K, Narita T, Sugiya H. JNK activation is essential for activation of MEK/ERK signaling in IL-1β-induced COX-2 expression in synovial fibroblasts. Scientific Rep 2017;7:39914.

[53] Lane NE, Schnitzer TJ, Birbara CA, Mokhtarani M, Shelton DL, Smith MD, Brown MT. Tanezumab for the treatment of pain from osteoarthritis of the knee. N Engl J Med 2010;363:1521–31.
[54] Larsson J, Ekblom A, Henriksson K, Lundeberg T, Theodorsson E. Concentration of substance p, neurokinin a, calcitonin gene-related peptide, neuropeptide y and vasoactive intestinal polypeptide in synovial fluid from knee joints in patients suffering from rheumatoid arthritis. Scand J Rheumatol 1991;20:326–35.
[55] Lo J, Chan L, Flynn S. A systematic review of the incidence, prevalence, costs, and activity and work limitations of amputation, osteoarthritis, rheumatoid arthritis, back pain, multiple sclerosis, spinal cord injury, stroke, and traumatic brain injury in the United States: a 2019 update. Arch Phys Med Rehabil 2021;102:115–31.
[56] Loeser RF, Erickson EA, Long DL. Mitogen-activated protein kinases as therapeutic targets in osteoarthritis. Curr Opin Rheumatol 2008;20:581–6.
[57] Loeser JD. Reliving pain in America. Clin J Pain 2012;28:185–6.
[58] Luo Y, Zheng SG. Hall of fame among pro-inflammatory cytokines: interleukin-6 gene and its transcriptional regulation mechanisms. Front Immunol 2016;7:604.
[59] Ma QP. The expression of bradykinin B1receptors on primary sensory neurones that give rise to small caliber sciatic nerve fibres in rats. Neuroscience 2001;107:665–73.
[60] Mandl LA. Osteoarthritis year in review 2018: clinical. Osteoarthritis Cartilage 2019;27:359–64.
[61] Manning DC, Raja SN, Meyer RA, Campbell JN. Pain and hyperalgesia after intradermal injection of bradykinin in humans. Clin Pharmacol Ther 1991;50:721–9.
[62] Mao Y, Zhou J, Liu X, Gu E, Zhang Z, Tao W. Comparison of different histone deacetylase inhibitors in attenuating inflammatory pain in rats. Pain Res Manag 2019;2019:1648919.
[63] Marceau F, Bachelard H, Bouthillier J, Fortin JP, Morissette G, Bawolak MT, Charest-Morin X, Gera L. Bradykinin receptors: agonists, antagonists, expression, signaling, and adaptation to sustained stimulation. Int Immunopharmacol 2020;82:106305.
[64] Matsuoka Y, Yang J. Selective inhibition of extracellular signal-regulated kinases 1/2 blocks nerve growth factor to brain-derived neurotrophic factor signaling and suppresses the development of and reverses already established pain behavior in rats. Neuroscience 2012;206:224–36.
[65] McDougall JJ, Watkins L, Li Z. Vasoactive intestinal peptide (VIP) is a modulator of joint pain in a rat model of osteoarthritis. PAIN 2006;123: 98–105.
[66] McGraw KO, Wong SP. A common language effect size statistic. Psychol Bull 1992;111:361–5.
[67] Meini S, Maggi CA. Knee osteoarthritis: a role for bradykinin? Inflamm Res 2008;57:351–61.
[68] Meves H. The action of prostaglandins on ion channels. Curr Neuropharmacol 2006;4:41–57.
[69] Miller RE, Miller RJ, Malfait AM. Osteoarthritis joint pain: the cytokine connection. Cytokine 2014;70:185–93.
[70] Moffat JG, Vincent F, Lee JA, Eder J, Prunotto M. Opportunities and challenges in phenotypic drug discovery: an industry perspective. Nat Rev Drug Discov 2017;16:531–43.
[71] Montanara PL, Hervera A, Baltussen LL, Hutson TH, Palmisano I, De Virgiliis F, Kong G, Chadwick J, Gao Y, Bartus K, Majid QA, Gorgoraptis N, Wong K, Downs J, Pizzorusso T, Ultanir SK, Leonard H, Yu H, Millar DS, Istvan N, Mazarakis ND, Giovanni SD. Cyclin-dependent-like kinase 5 is required for pain signaling in human sensory neurons and mouse models. Sci Transl Med 2020;12:eaax4846.
[72] Moriyama T, Higashi T, Togashi K, Iida T, Segi E, Sugimoto Y, Tominaga T, Narumiya S, Tominaga M. Sensitization of TRPVI by EP1 and IP reveals peripheral nociceptive mechanism of prostaglandins. Mol Pain 2005;1:3. doi: 10.1186/1744-8069-1-3.
[73] Mukamel EA, Nimmerjahn A, Schnitzer MJ. Automated analysis of cellular signals from large-scale calcium imaging data. Neuron 2009;63: 747–60.
[74] Munro G, Dalby-Brown W. Kv7 (KCNQ) channel modulators and neuropathic pain. J Med Chem 2007;50:2576–82.
[75] Murphy L, Helmick CG. The impact of osteoarthritis in the United States: a population-health perspective. Am J Nurs 2012;112:S13–9.
[76] Namer B, Schmidt D, Eberhardt E, Maroni M, Dorfmeister E, Kleggetveit IP, Kaluza L, Meents J, Gerlach A, Lin Z, Winterpacht A, Dragicevic E, Kohl Z, Schüttler J, Kurth I, Warncke T, Jorum E, Winner B, Lampert A. Pain relief in a neuropathy patient by lacosamide: proof of principle of clinical translation from patient-specific iPS cell-derived nociceptors. EBioMedicine 2019;39:401–8.
[77] Nees TA, Rosshirt N, Zhang JA, Reiner T, Sorbi R, Tripel E, Walker T, Schiltenwolf M, Hagmann S, Moradi B. Synovial cytokines significantly correlate with osteoarthritis-related knee pain and disability: inflammatory mediators of potential clinical relevance. J Clin Med 2019;8:1343.
[78] Nguyen C, Upadhyay H, Murphy M, Borja G, Rozsahegyi EJ, Barnett A, Brookings T, McManus OB, Werley CA. Simultaneous voltage and calcium imaging and optogenetic stimulation with high sensitivity and a wide field of view. Biomed Opt Express 2019;10:789.
[79] Nucifora FC, Mihaljevic M, Lee BJ, Sawa A. Clozapine as a model for antipsychotic development. Neurotherapeutics 2017;14:750–61.
[80] Obreja O, Rathee PK, Lips KS, Distler C, Kress M. IL-1 beta potentiates heat-activated currents in rat sensory neurons: involvement of IL-1RI, tyrosine kinase, and protein kinase C. FASEB J 2002;16:1497–503.
[81] Obreja O, Biasio W, Andratsch M, Lips KS, Rathee PK, Ludwig A, Rose-John S, Kress M. Fast modulation of heat-activated ionic current by proinflammatory interleukin 6 in rat sensory neurons. Brain 2005;128: 1634–41.
[82] Passmore G, Delmas P. Does cure for pain REST on Kv7 channels? PAIN 2011;152:709–10.
[83] Payne CE, Brown AR, Theile JW, Loucif AJC, Alexandrou AJ, Fuller MD, Mahoney JH, Antonio BM, Gerlach AC, Printzenhoff DM, Prime RL, Stockbridge G, Kirkup AJ, Bannon AW, England S, Chapman ML, Bagal S, Roeloffs R, Anand U, Anand P, Bungay PJ, Kemp M, Butt RP, Stevens EB. A novel selective and orally bioavailable Nav1.8 channel blocker, PF-01247324, attenuates nociception and sensory neuron excitability. Br J Pharmacol 2015;172:2654–70.
[84] Pinto LG, Cunha TM, Vieira SM, Lemos HP, Verri WA, Cunha FQ, Ferreira SH. IL-17 mediates articular hypernociception in antigen-induced arthritis in mice. PAIN 2010;148:247–56.
[85] Qiu F, Jiang Y, Zhang H, Liu Y, Mi W. Increased expression of tetrodotoxin-resistant sodium channels Nav1. 8 and Nav1. 9 within dorsal root ganglia in a rat model of bone cancer pain. Neurosci Lett 2012;512:61–6.
[86] Rae GA, Calixto JB. Interactions of calcium antagonists and the calcium channel agonist Bay K 8644 on neurotransmission of the mouse isolated vas deferens. Br J Pharmacol 1989;96:333–40.
[87] Rahmati M, Mobasheri A, Mozafari M. Inflammatory mediators in osteoarthritis: a critical review of the state-of-the-art, current prospects, and future challenges. Bone 2016;85:81–90.
[88] Ray P, Torck A, Quigley L, Wangzhou A, Neiman M, Rao C, Lam T, Kim J-Y, Kim TH, Zhang MQ, Dussor G, Price TJ. Comparative transcriptome profiling of the human and mouse dorsal root ganglia: an RNA-seq–based resource for pain and sensory neuroscience research. PAIN 2018;159:1325–45.
[89] Richter F, Natura G, Löser S, Schmidt K, Viisanen H, Schaible HG. Tumor necrosis factor causes persistent sensitization of joint nociceptors to mechanical stimuli in rats. Arthritis Rheum 2010;62: 3806–14.
[90] Richter F, Natura G, Ebbinghaus M, Von Banchet GS, Hensellek S, König C, Bräuer R, Schaible HG. Interleukin-17 sensitizes joint nociceptors to mechanical stimuli and contributes to arthritic pain through neuronal interleukin-17 receptors in rodents. Arthritis Rheum 2012;64:4125–34.
[91] Rickert V, Kramer D, Schubert A-L, Sommer C, Wischmeyer E, Üçeyler N. Globotriaosylceramide-induced reduction of KCa1.1 channel activity and activation of the Notch1 signaling pathway in skin fibroblasts of male Fabry patients with pain. Exp Neurol 2020;324:113134.
[92] Roberts PJ, Der CJ. Targeting the Raf-MEK-ERK mitogen-activated protein kinase cascade for the treatment of cancer. Oncogene 2007;26: 3291–310.
[93] Ruiz-Negrón N, Menon J, King JB, Ma J, Bellows BK. Cost-Effectiveness of treatment options for neuropathic pain: a systematic review. Pharmacoeconomics 2019;37:669–88.
[94] Sanger GJ, Ellis ES, Harries MH, Tilford NS, Wardle KA, Benham CD. Rank-order inhibition by ømega-conotoxins in human and animal autonomic nerve preparations. Eur J Pharmacol 2000;388: 89–95.
[95] Schepman P, Thakkar S, Robinson R, Malhotra D, Emir B, Beck C. Moderate to severe osteoarthritis pain and its impact on patients in the United States: a national survey. J Pain Res 2021;14: 2313–26.
[96] Schuelert N, McDougall JJ. Electrophysiological evidence that the vasoactive intestinal peptide receptor antagonist VIP6-28 reduces nociception in an animal model of osteoarthritis. Osteoarthritis Cartilage 2006;14:1155–62.
[97] Segond von Banchet G, Boettger MK, König C, Iwakura Y, Bräuer R, Schaible HG. Neuronal IL-17 receptor upregulates TRPV4 but not TRPV1 receptors in DRG neurons and mediates mechanical but not thermal hyperalgesia. Mol Cell Neurosci 2013;52:152–60.

[98] Serrano A, Paré M, McIntosh F, Elmes SJR, Martino G, Jomphe C, Lessard E, Lembo PMC, Vaillancourt F, Perkins MN, Cao CQ. Blocking spinal CCR2 with AZ889 reversed hyperalgesia in a model of neuropathic pain. Mol Pain 2010;6:90.
[99] Shiers S, Mwirigi J, Pradhan G, Kume M, Black B, Barragan-Iglesias P, Moy JK, Dussor G, Pancrazio JJ, Kroener S, Price TJ. Reversal of peripheral nerve injury-induced neuropathic pain and cognitive dysfunction via genetic and tomivosertib targeting of MNK. Neuropsychopharmacology 2020;45:524–33.
[100] Shu X, Mendell LM. Nerve growth factor acutely sensitizes the response of adult rat sensory neurons to capsaicin. Neurosci Lett 1999;274: 159–62.
[101] Song IH, Althoff CE, Hermann KG, Scheel AK, Knetsch T, Burmester GR, Backhaus M. Contrast-enhanced ultrasound in monitoring the efficacy of a bradykinin receptor 2 antagonist in painful knee osteoarthritis compared with MRI. Ann Rheum Dis 2009;68:75–83.
[102] St Sauver JL, Warner DO, Yawn BP, Jacobson DJ, McGree ME, Pankratz JJ, Melton LJ, Roger VL, Ebbert JO, Rocca WA, Rocca WA. Why patients visit their doctors: assessing the most prevalent conditions in a defined American population. Mayo Clinic Proc 2013;88:56–67.
[103] Stamboulian S, Choi J-S, Ahn H-S, Chang Y-W, Tyrrell L, Black JA, Waxman SG, Dib-Hajj SD. ERK1/2 mitogen-activated protein kinase phosphorylates sodium channel Nav1. 7 and alters its gating properties. J Neurosci 2010;30:1637–47.
[104] Stas JI, Bocksteins E, Jensen CS, Schmitt N, Snyders DJ. The anticonvulsant retigabine suppresses neuronal KV 2-mediated currents. Scientific Rep 2016;6:35080.
[105] Steen KH, Steen AE, Kreysel H-W, Reeh PW. Inflammatory mediators potentiate pain induced by experimental tissue acidosis. PAIN 1996;66: 163–70.
[106] Stevens SM, McClelland CM, Trusheim JE, Lee MS. Carboplatin-associated cranial neuropathy. Neuroophthalmology 2018;42:302–5.
[107] Su Y-S, Sun W-H, Chen C-C. Molecular mechanism of inflammatory pain. World J Anesthesiol 2014;3:71–81.
[108] Sun JH, Yang B, Donnelly DF, Ma C, LaMotte RH. MCP-1 enhances excitability of nociceptive neurons in chronically compressed dorsal root ganglia. J Neurophysiol 2006;96:2189–99.
[109] Sutton S, Clutterbuck A, Harris P, Gent T, Freeman S, Foster N, Barrett-Jolley R, Mobasheri A. The contribution of the synovium, synovial derived inflammatory cytokines and neuropeptides to the pathogenesis of osteoarthritis. Vet J 2009;179:10–24.
[110] Swinney DC, Anthony J. How were new medicines discovered? Nat Rev Drug Discov 2011;10:507–19.
[111] Tibshirani R. Regression shrinkage and selection via the lasso. J R Stat Soc Ser B (Methodological) 1996;58:267–88.
[112] Vaudry D, Stork PJS, Lazarovici P, Eiden LE. Signaling pathways for PC12 cell differentiation: making the right connections. Science 2002; 296:1648–9.
[113] Wang D, DuBois RN. Role of prostanoids in gastrointestinal cancer. J Clin Invest 2018;128:2732–42.
[114] Watkins LR, Wiertelak EP, Goehler LE, Smith KP, Martin D, Maier SF. Characterization of cytokine-induced hyperalgesia. Brain Res 1994; 654:15–26.
[115] Werley CA, Brookings T, Upadhyay H, Williams LA, McManus OB, Dempsey GT. All-optical electrophysiology for disease modeling and pharmacological characterization of neurons. Curr Protoc Pharmacol 2017;78:11.20.1–24.
[116] Werley CA, Chien M-P, Cohen AE. Ultrawidefield microscope for high-speed fluorescence imaging and targeted optogenetic stimulation. Biomed Opt Express 2017;8:5794.
[117] Williams LA, Joshi V, Murphy M, Ferrante J, Werley CA, Brookings T, McManus O, Grosse J, Davies CH, Dempsey GT. Scalable measurements of intrinsic excitability in human iPS cell-derived excitatory neurons using all-optical electrophysiology. Neurochem Res 2019;44:714–25.
[118] Woolf CJ. Overcoming obstacles to developing new analgesics. Nat Med 2010;16:1241–7.
[119] Xu M, Wang Y, Xia R, Wei Y, Wei X. Role of the CCL2-CCR2 signalling axis in cancer: mechanisms and therapeutic targeting. Cell Prolif 2021; 54:e13115.
[120] Yam MF, Loh YC, Oo CW, Basir R. Overview of neurological mechanism of pain profile used for animal "pain-like" behavioral study with proposed analgesic pathways. Int J Mol Sci 2020;21:4355.
[121] Yu H, Wu M, Townsend SD, Zou B, Long S, Daniels JS, McManus OB, Li M, Lindsley CW, Hopkins CR. Discovery, synthesis, and structure activity relationship of a series of N-aryl- bicyclo[2.2.1]heptane-2-carboxamides: characterization of ML213 as a novel KCNQ2 and KCNQ4 potassium channel opener. ACS Chem Neurosci 2011;2:572–7.
[122] Yu H, Wu M, Hopkins C, Engers J, Townsend S, Lindsley C, McManus OB, Li M. A small molecule activator of KCNQ2 and KCNQ4 channels. Probe reports from the NIH molecular libraries program, 2013. Available at: https://www.ncbi.nlm.nih.gov/books/NBK133435/. Accessed October 26, 2021.
[123] Zhang H, Cohen AE. Optogenetic approaches to drug discovery in neuroscience and beyond. Trends Biotechnol 2017;35:625–39.
[124] Zhang W, Liu HT. MAPK signal pathways in the regulation of cell proliferation in mammalian cells. Cell Res 2002;12:9–18.
[125] Zhang F-X, Gadotti VM, Souza IA, Chen L, Zamponi GW. BK potassium channels suppress Cavα2δ subunit function to reduce inflammatory and neuropathic pain. Cell Rep 2018;22:1956–64.
[126] Zheng W, Thorne N, McKew JC. Phenotypic screens as a renewed approach for drug discovery. Drug Discov Today 2013;18:1067–73.